发 光 学 报
CHINESE JOURNAL OF LUMINESCENCE

Article ID: 1000-7032(XXXX)XX-0001-28

CPL-Active Inorganic Nanomaterials: Synthetic Strategies and Applications

ZHOU Binqian[1,2], LEI Qian[1,2], ZHANG Zhitao[1,2], WANG Rui[1,2], HAO Junjie[2*], CHENG Jiaji[1*], JIA Tingting[1*]

(1. *School of Materials Science and Engineering, Hubei University, Wuhan* 430062, *China*;
2. *College of Integrated Circuits and Optoelectronic Chips, Shenzhen Technology University, Shenzhen* 518118, *China*)

* *Corresponding Authors, E-mail: haojunjie@sztu. edu. cn; jiajicheng@hubu. edu. cn; jia. tingting@hubu. edu. cn*

Abstract: CPL-active inorganic quantum dots have emerged as a rapidly developing class of chiral nanomaterials that combine excellent photophysical properties with unique chiroptical activity. According to the chirality induction pathway, the synthesis strategies of CPL-active inorganic quantum dots can generally be classified into two universal categories: one-step synthesis and two-step synthesis. Each strategy presents distinct advantages and limitations in balancing crystal quality, fluorescence efficiency, and chiroptical performance. This review systematically summarizes recent progress in the synthesis and applications of CPL-active inorganic quantum dots, with particular emphasis on chiral semiconductor quantum dots, chiral carbon dots, and chiral perovskites. Their emerging applications in circularly polarized photodetectors, chiral sensing, spintronics, and next-generation optoelectronic devices are also envisioned. Finally, current challenges and future opportunities for the rational design of high-performance CPL-active inorganic nanomaterials are highlighted, aiming to provide guidance for the development of future chiral photonic and spin-optoelectronic systems.

Keywords: CPL; inorganic quantum dots; circularly polarized photodetectors; chiral sensing

CLC number: O482. 31 **Document code**: A

DOI: 10. 37188/CJL. 20260160 **CSTR**: 32170. 14. CJL. 20260160

CPL活性无机纳米材料:合成策略与应用

周宾倩[1,2], 雷茜[1,2], 张志涛[1,2], 王锐[1,2], 郝俊杰[2*], 程佳吉[1*], 贾婷婷[1*]

(1.湖北大学, 材料科学与工程学院, 武汉 430062;
2.深圳技术大学, 集成电路与光电芯片学院, 深圳 518118)

摘要: CPL活性无机量子点作为一类快速发展的手性纳米材料,近年来受到广泛关注。这类材料兼具优异的光物理性质与独特的手性光学活性。根据手性诱导路径的不同,CPL活性无机量子点的合成策略通常可分为两大类:一步合成法和两步合成法。两种策略在晶体质量、荧光效率与手性光学性能之间的平衡方面各具优势与局限性。本综述系统总结了近年来CPL活性无机量子点在合成与应用方面的研究进展,重点关注手性半导体量子点、手性碳点以及手性钙钛矿材料。同时,还总结了其在圆偏振光探测器、手性传感、自旋电子学以及新一代光电器件等领域的潜在应用。最后,本文对高性能CPL活性无机纳米材料的理性设计所面临的挑战与未来发展机遇进行了总结与展望,旨在为未来手性光子学与自旋光电子学体系的发展提供指导。

关 键 词: 圆偏振发光; 无机量子点; 圆偏振光电探测器; 手性传感

收稿日期: 2020-01-03; **修订日期**: 2020-01-05
基金项目: 国家自然科学基金(62261136552, 62204107)
Supported by National Natural Science Foundation of China(62261136552, 62204107)

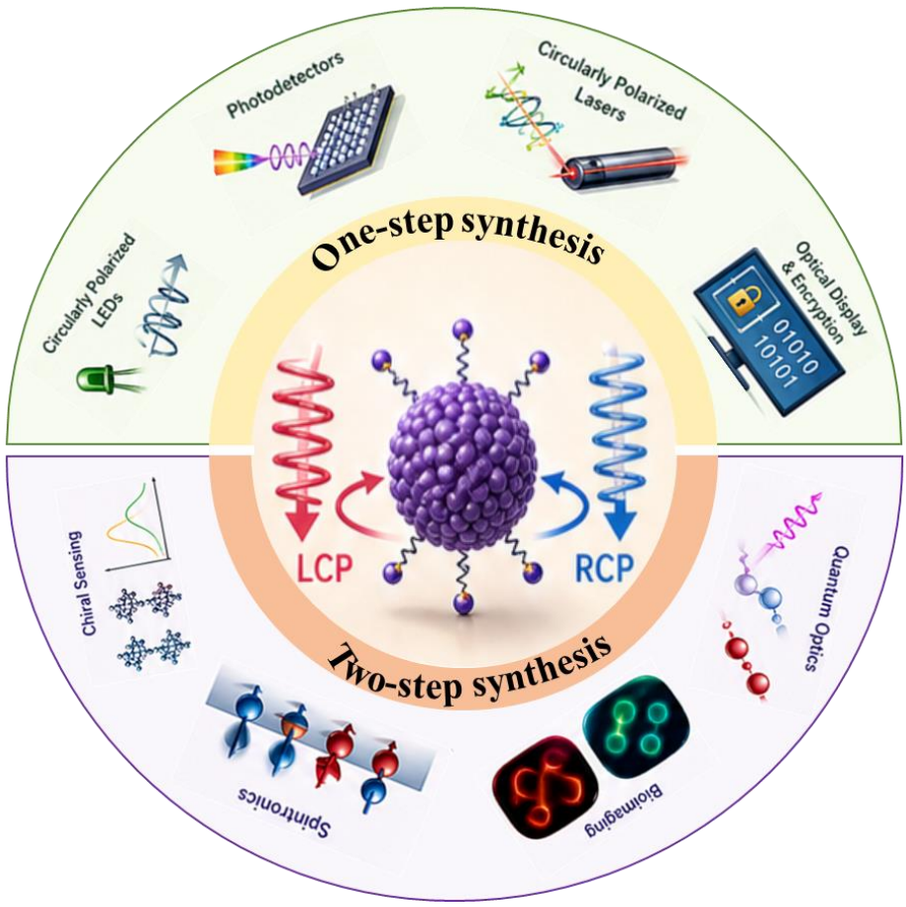

1 Introduction

Circularly polarized luminescence (CPL)-active inorganic nanomaterials have attracted extensive attention in recent years as an emerging class of chiral nanomaterials with both featured photophysical properties and unique chiroptical activity[1-3]. Chirality is a fundamental structural property in which two objects exist as non-superimposable mirror images, commonly referred to as left- and right-handed enantiomers[4]. In optical systems, chirality gives rise to characteristic phenomena such as circular dichroism (CD) and CPL, which originate from the differential interaction of materials with left-handed circularly polarized light (LCPL) and right-handed circularly polarized light (RCPL)[5]. These chiroptical properties are of great significance for a wide range of applications, including enantioselective recognition[6], 3D imaging[7], spintronics[8], circularly polarized photodetection[9], optical information encryption[10], and next-generation optoelectronic devices[11].

Compared with traditional chiral organic molecules, inorganic nanomaterials possess several intrinsic advantages, including size-dependent bandgap tunability, high photoluminescence quantum

yield, high photostability, and superior charge transport properties[12]. More importantly, the introduction of chirality into quantum-confined semiconductor nanostructures enables the combination of strong excitonic emission with spin-selective optical transitions, thereby providing an ideal platform for high-performance CPL materials. In addition to conventional II – VI and III – V semiconductor quantum dots such as CdSe, CdS, and InP, carbon dots and metal halide perovskite nanocrystals have also emerged as important CPL-active inorganic nanomaterials due to their excellent luminescence properties, structural diversity, and versatile chirality induction pathways[13].

Recent reviews on CPL-active inorganic nanomaterials have mainly focused on specific material systems or application fields[14, 15]. In contrast, this review adopts a synthesis-strategy-oriented framework based on one-step and two-step approaches. Despite

the significant differences in crystal structures and compositions, the synthesis strategies of CPL-active inorganic quantum dots can generally be summarized into two universal categories: one-step synthesis and two-step synthesis, because the synthetic route directly influences chirality induction pathways, surface structures, optical properties, and scalability of inorganic quantum dots, shown in Table 1. This classification not only provides a clear and universal perspective for comparing different material systems, including semiconductor quantum dots, carbon dots, and perovskite nanocrystals, but also helps to elucidate the intrinsic trade-offs between crystal quality, photoluminescence efficiency, and chiroptical performance. One-step synthesis refers to the direct introduction of chiral sources during the nucleation and growth of nanocrystals, allowing chirality to be generated simultaneously with the formation of the nanoparticle's framework. Typical examples include the direct aqueous-phase synthesis of chiral CdS quantum dots using penicillamine (Pen) as capping ligands[16], hydrothermal carbonization of amino-acid-derived precursors for chiral carbon dots[17], and direct crystallization of chiral perovskites using chiral organic ammonium salts[18]. This strategy is simple and efficient and often produces strong chirality transfer, but it may suffer from poor control over crystal quality, broad emission spectra, and relatively low fluorescence quantum yields. In contrast, two-step synthesis involves the initial preparation of high-quality achiral cores, followed by post-synthetic chirality induction through ligand exchange, surface functionalization, interface-mediated coordination growth, or supramolecular self-assembly. This approach not only preserves the excellent optical properties of the original quantum dots but also provides greater flexibility for tuning chiroptical performance. In some cases, interface-mediated coordination growth can further overcome shell-screening effects and significantly strengthen orbital hybridization between chiral ligands and semiconductor cores, leading to remarkably enhanced luminescence dissymmetry factors[19, 20].

Table 1 Comparison of one-step and two-step synthesis strategies for CPL-active inorganic nanomaterials

Synthesis Strategy	Mechanism	Typical Methods	Advantages / Limitations	Application Scenarios	Ref.
One-step synthesis	Chirality is introduced during nucleation and growth of nanocrystals; chiral ligands or precursors directly participate in crystal formation	Direct aqueous synthesis with chiral ligands Hydrothermal carbonization Direct crystallization of chiral perovskites	· Simple and efficient process · Strong chirality transfer Potential intrinsic chirality · Poor control over crystal quality · Broad emission spectra · Lower PLQY Surface defects are common	low-cost and mass-producible materials (display technologies)	33-41 73-74 91-93
Two-step synthesis	High-quality achiral nanocrystals are first synthesized, followed by post-synthetic chirality induction via surface modification or assembly	Ligand exchange Surface functionalization Template-induced assembly	· Preserves high optical quality · Flexible and tunable · Better control of PLQY · Compatible with complex nanostructures · Weaker electronic coupling · Possible reduction in chiroptical signals · Additional processing steps required	High luminescence efficiency, tunable CPL responses, or precise surface functionality (biosensing, chiral recognition)	42-53 75-80 94-98
	Chirality introduced during shell growth via interfacial coordination	Oil/water interface coordination growth Ligand - metal complex-assisted shell formation	· Strong chirality and high PLQY · Enhanced core - ligand coupling · More complex synthesis · Limited universality		19

Herein, this review systematically summarizes recent advances in the synthesis strategies and applications of CPL-active inorganic quantum dots, with particular focus on chiral semiconductor quantum dots, chiral carbon dots, and chiral perovskites. Emphasis is placed on the universal one-step and two-step synthetic approaches and their practical applications in circularly polarized photodetectors, chiral sensing and spintronic devices. Finally, the current challenges and future perspectives for the rational design of high-performance CPL-active inorganic quantum dots are discussed. This review aims to provide a comprehensive understanding of the structure and application relationships in chiral semiconductor nanomaterials and to offer guidance for the development of next-generation chiral optoelectronic systems.

2 Chiral optical properties

2.1 Circular Dichroism

When plane-polarized light passes through a medium, if the two circularly polarized components propagate at the same velocity, the vibration direction remains unchanged. Such a medium is defined as optically inactive, i. e. , an achiral substance. In contrast, if the two circularly polarized components propagate at different velocities after passing through the medium, the superposition of these components leads to a change in the vibration direction of the polarized light, and the medium is therefore considered optically active[21]. The optical activity of chiral materials can be mainly classified into two types: optical rotatory dispersion (ORD) and CD. These properties are typically measured using an optical rotatory dispersion spectrometer and a circular dichroism spectrometer, respectively. Among them, circular dichroism is particularly useful for reflecting the optical characteristics of chiral substances and is widely employed in the study of their structures. Since the discovery of circular dichroism in 1895 by the French physicist Cotton in aqueous solutions of copper (II) and copper (III) tartrate complexes, circular dichroism spectroscopy has been widely applied in chemistry, biology, agriculture, and other fields, greatly advancing the study of chirality.

CD refers to the differential absorption of LCPL and RCPL by optically active molecules. This phenomenon occurs because an enantiomeric or chiral medium exhibits distinct absorption coefficients for these two components[22]. When incident LCPL and RCPL of equal amplitude pass through such a medium, the disparity in absorption causes the resulting light to become elliptically polarized[23, 24]. The degree of this ellipticity, denoted as θ, is defined by the ratio of the minor axis to the major axis of the resultant ellipse. Mathematically, it can be expressed as:

$$\theta = \arctan\left(\frac{b}{a}\right) = \arctan\left(\frac{E_R - E_L}{E_R + E_L}\right) \#(1)$$

where a and b represent the semi-major and semi-minor axes, respectively, while E_R and E_L denote the amplitudes of the right- and left-handed circularly polarized light after passing through the sample. Furthermore, the amplitude is intrinsically related to the absorption coefficient k and the optical path length l through the medium, expressed as $E_l = E_0 e^{-2\pi kl/\lambda}$. By substituting this relationship into the aforementioned equation, the ellipticity can be rewritten as:

$$\theta = \arctan\left(\frac{e^{-2\pi k_R l/\lambda} - e^{-2\pi k_L l/\lambda}}{e^{-2\pi k_R l/\lambda} + e^{-2\pi k_L l/\lambda}}\right) = \frac{\pi l}{\lambda}\left(k_L - k_R\right) \#(2)$$

where k_L and k_R represent the absorption coefficients for left- and right-handed circularly polarized light, respectively. It can be observed that the ellipticity is a function of Δk, which constitutes the CD mentioned previously. Currently, the molar extinction coefficient of circularly polarized light is commonly used to calculate ellipticity, which is defined according to the Beer – Lambert law as:

$$\varepsilon = \frac{1}{cl} \lg \frac{I_0}{I_l} \#(3)$$

where ε is the molar extinction coefficient, c is the solution concentration, l is the optical path length, I_0 is the incident light intensity, and I_l is the transmitted light intensity. The most widely used expression for calculating ellipticity is derived from mathematical transformations relating light intensity, ampli-

tude, and extinction coefficients, and can be written as:

$$[\theta] = 3300(\varepsilon_L - \varepsilon_R) = 3300\Delta\varepsilon \#(4)$$

where 3300 is the standard conversion factor.

2.2 Circularly Polarized luminescence

CPL is a special form of polarized light in which the electric field vector rotates with time in a plane perpendicular to the direction of propagation, tracing a circular trajectory. When light propagates along a certain direction, if the endpoint of the electric field vector rotates uniformly with time in the plane perpendicular to the propagation direction while maintaining a constant amplitude, the light is defined as circularly polarized[25-27]. According to the rotation direction of the electric field vector, CPL can be classified into LCPL and RCPL. Conventionally, when an observer faces the direction of light propagation, counterclockwise rotation of the electric field vector corresponds to LCPL, while clockwise rotation corresponds to RCPL. From the perspective of electromagnetic wave theory, light is a transverse wave in which both the electric field vector E and the magnetic field vector B are perpendicular to the direction of propagation[28]. Assuming that light propagates along the z direction, the electric field can be decomposed into two orthogonal components, E_x and E_y, vibrating along the x and y directions, respectively. In general, linearly polarized light can be described as vibration along a single direction. If an additional orthogonal component is introduced with the same amplitude and a phase difference of $\pi/2$, circularly polarized light can be generated. The electric field components can then be expressed as:

$$E_x = E_0 \cos(kz - \omega t) \#(5)$$

$$E_y = E_0 \sin(kz - \omega t) \#(6)$$

where $E_0$is the electric field amplitude, $k$is the wave vector, $\omega$is the angular frequency, and $t$is time. By combining these two components, the time evolution of the electric field vector can be written as:

$$E_x^2 + E_y^2 = E_0^2 \#(7)$$

This equation indicates that, at any fixed propagation position z, the endpoint of the electric field vector satisfies the equation of a circle. Therefore, the electric field undergoes uniform circular motion in the plane, which is the essential characteristic of circularly polarized light. CPL is related to the excited-state properties of chiral systems. In experimental optical systems, the most common method to generate CPL is by using a quarter-wave plate. When linearly polarized light is incident at an angle of 45° relative to the optical axis of the wave plate, the plate introduces a phase delay of $\pi/2$ between the two orthogonal components. As a result, the initially in-phase components acquire a quarter-period phase difference, ultimately forming circularly polarized light. In addition, CPL can also be directly generated from chiral luminescent materials. The difference in emission intensity between left- and right-handed circularly polarized light is commonly used to quantify CPL, which can be expressed as:

$$\Delta I = I_L - I_R \#(8)$$

where $I_L$and I_R represent the emission intensities of L-CPL and R-CPL, respectively. The quality of CPL can be evaluated using the luminescence dissymmetry factor, defined as:

$$g_{\mathrm{lum}} = \frac{I_L - I_R}{\frac{1}{2}(I_L + I_R)} = \frac{2(I_L - I_R)}{I_L + I_R} \#(9)$$

In quantum optics and studies of light – matter interactions, circularly polarized light plays an important role. Owing to its well-defined chiral rotation of the electric field vector, it carries rich optical information and lacks angular dependence, making it applicable in quantum computing, satellite communication, asymmetric synthesis, and magnetic recording[29-32].

It is worth emphasizing that CD and CPL originate from different electronic processes and therefore do not necessarily appear simultaneously. In inorganic quantum dots, CD is often associated with chiral surface coordination, lattice distortion, or chiral superstructures, while CPL depends more directly on the chirality of emissive excitonic states and radiative transition pathways[2]. Therefore, although CD and CPL are closely related manifestations of chirality, there is no strict one-to-one correspondence between them.

3 Chiral semiconductor Quantum Dots

3.1 Direct Synthesis

In 2007, Gun′ko and co-workers reported the first example of chiral semiconductor nanomaterials[16]. Under microwave-assisted conditions, CdS QDs were directly synthesized using L-/D-Pen as stabilizing ligands. This work demonstrated, for the first time, that chiral ligands can directly induce CD signals in inorganic semiconductor nanocrystal cores, thereby breaking the conventional notion that chirality is restricted to organic molecules or metallic clusters. And pronounced mirror-image CD signals were observed for products (Figure 1A). CdS cores are intrinsically achiral, the authors proposed that the optical activity originates from the interactions between the quantum dot surface and the chiral ligands. Then they confirmed this hypothesis through density functional theory (DFT) calculations[33]. Their results revealed that Pen ligands can significantly distort the spatial arrangement of surface atoms, leading to the formation of chiral surface structures. Specifically, L-/D-Pen binds to surface metal atoms *via* N and S atoms, while the carboxylate group coordinates with neighboring surface sites, collectively introducing asymmetry into the nanocrystal surface. In 2010, Gun′ko's group further extended this strategy by synthesizing tetrapod-shaped CdS nanocrystals through refluxing penicillamine in alkaline aqueous solutions[34]. This work represented one of the earliest attempts to introduce chirality into nanocrystals with complex morphologies. Although the CD signals of these tetrapod-shaped CdS were relatively weak, the materials exhibited excellent biocompatibility. Notably, even at concentrations as high as 40 μg mL^{-1}, the nanocrystals maintained high viability (>90%) in NG108-15 cells (Figure 1B), demonstrating that surface passivation by chiral ligands effectively suppresses Cd^{2+} ion leakage. This finding highlights their potential for applica-

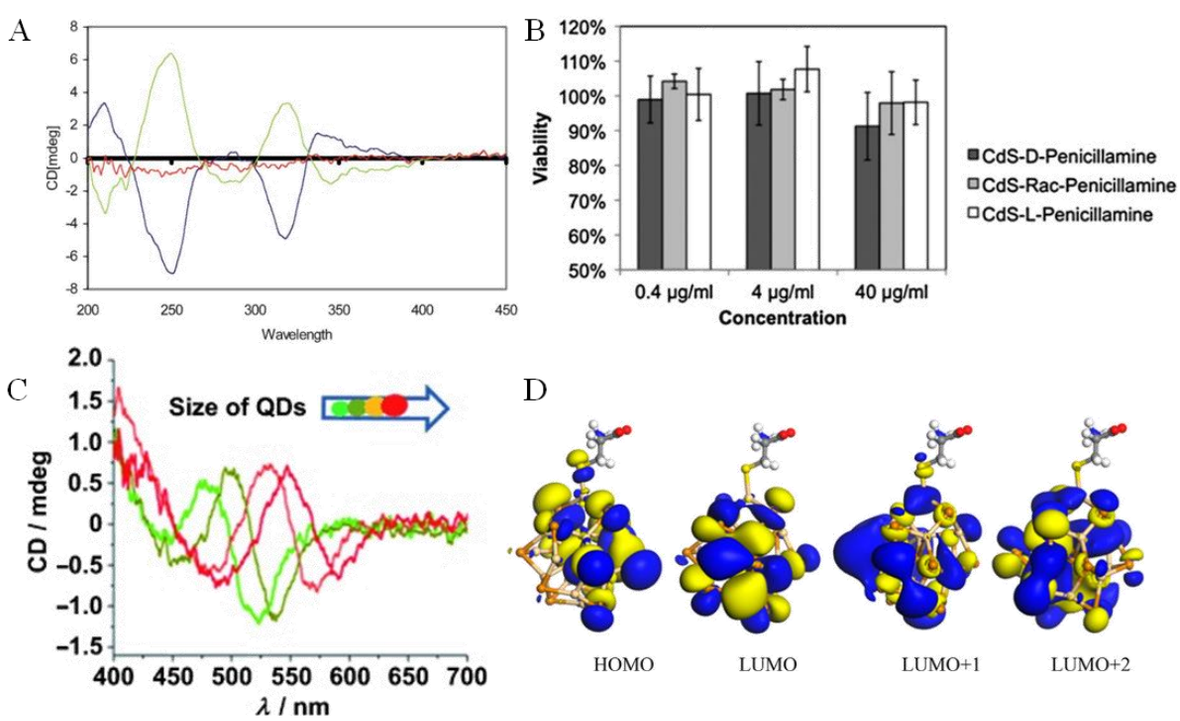

Figure 1 (A) CD scans of the D-/L- / Rac-Pen stabilized CdS QDs[16]. (reproduced from ref. 16 with permission from Royal Society of Chemistry). (B) Histograms showing the evaluation of cell viability depending on tetrapod concentration[34]. (reproduced from ref. 34 with permission from Royal Society of Chemistry). (C) QDs stabilized by chiral biomolecules show size-dependent CD characteristics in the visible light region[36]. (reproduced from ref. 36 with permission from Wiley). (D) Calculated molecular orbital of L-Cys-$(CdTe)_{13}$[39]. (reproduced from ref. 39 with permission from American Chemical Society).

tions in chiral biosensing and cellular imaging. In 2010, their recent work used chiral ligands L-/D-Cys to regulate the nucleation and growth of CdTe QDs. They proposed a topological origin model of chiral centers on the surface of inorganic nanocrystals at the atomic level[35]. They also found that chiral ligands exert a stereoselective influence on the growth kinetics of nanocrystals. Experimental results showed that CdTe QDs stabilized by L-Cys exhibited a faster growth rate, which was attributed to the thermodynamic preference of chiral ligands for selectively stabilizing specific surface facets. In 2011, Tang *et al.* also prepared a series of CdTe QDs with sizes ranging from 2.7 to 4.2 nm through a one-pot synthesis method by precisely controlling the reaction time[36]. It was found that the CD peak position shifted synchronously with the first excitonic absorption peak, and the g-factor decreased with increasing size (Figure 1C). Different from the mainstream view at that time that chirality only originated from surface defects or the ligands themselves, they proposed that chirality arose from the electric dipole – dipole coupling between chiral molecules and quantum dots, rather than from the simple contribution of ligands. The hybridization between ligand molecular orbitals and QD electronic states leads to asymmetric transition dipoles, giving rise to CD and CPL signals. This theoretically explained why CD signals could be observed in the visible region where the ligands themselves expressed no absorption activity. Moreover, these findings collectively overturned the earlier conclusion that achiral semiconductor cores cannot exhibit optical activity. Rather, they demonstrated that the interplay between surface chemistry and electronic structure can effectively transfer and amplify chirality from molecular ligands to inorganic nanocrystals, establishing a new paradigm for the design of chiral semiconductor nanomaterials. At this point, a mature theoretical framework for the aqueous synthesis of semiconductor quantum dots had been established. Then researchers shifted their focus to deeper mechanistic studies and the potential applications of chiral semiconductor QDs in optical and biological fields[37, 38]. For example, unlike previous reports that mainly focused on the interaction between intrinsically chiral quantum dots and their chiral ligands, Yang et al. further advanced the understanding of the fundamental mechanism of chiral induction in semiconductor QDs by investigating the interactions between the surfaces of QDs and other chiral groups[39]. They found that the effects of added chiral molecules on the chiroptical signals and fluorescence of chiral CdTe were significantly chiral selective. Specifically, only when chiral molecules containing a thiol group (-SH) was introduced did the fluorescence and CD signals of L/D-Cys-CdTe QDs show a significant red shift, whereas chiral molecules without -SH did not cause such a red shift. Through experiments and DFT calculations, the authors attributed this phenomenon to the orbital hybridization between the highest occupied molecular orbital of -SH in cysteine and the valence band of CdTe QDs, which reduced the effective band gap (Figure 1D). In addition to chiral semiconductor QDs in the visible region, near-infrared chiral semiconductor QDs also have great application potential due to their deep tissue penetration and low autofluorescence[40]. Qu et al. successfully prepared chiral Ag_2S QDs with near-infrared fluorescence emission (~1060 nm) and chiroptical activity by a one-pot aqueous synthesis method[41]. Their study revealed that chirality has a significant influence on the molecular interactions between quantum dots and biological systems. They found that the selective accumulation of D-Ag_2S QDs in tumor regions was significantly higher than that of L-Ag_2S QDs. This difference was attributed to the chirality-dependent protein corona, which further influenced the interactions between the probes and the tumor microenvironment. This work provided a new strategy for regulating their biological behaviors, such as tumor targeting and toxicity, through rational engineering of their surface properties.

3.2 Post-synthetic Chirality Induction

Before 2013, the mainstream strategy for preparing chiral semiconductor nanocrystals was direct aqueous-phase synthesis, in which water-soluble chiral ligands were introduced during the nucleation

and growth stages of nanocrystals. In this approach, chiral ligands served as one of the starting reagents and directly coordinated with the quantum dot surface during crystal growth, thereby inducing chiroptical activity. In contrast to one-step approaches, two-step synthesis provides a more flexible and controllable route, where high-quality achiral nanocrystals are first prepared, followed by post-synthetic chirality induction through surface modification or assembly processes. A major breakthrough was reported by Balaz's group in 2013, who demonstrated the preparation of chiroptical activity CdSe QDs through post-synthetic ligand exchange[42]. Through this strategy, the original achiral surface ligands TOPO/OA were replaced by L/D-Cys, enabling originally achiral CdSe QDs to exhibit distinct CD signals in the visible region, as shown in Figure 2A. This represented the first application of post-synthetic ligand exchange in the preparation of chiral semiconductor QDs. The strategy provided a more flexible post-functionalization route compared with direct aqueous synthesis, while maintaining compatibility with high quality nanocrystals. In the same year, this group further reported that simple surface modification with chiral organic ligands could induce pronounced CPL in CdSe QDs[43]. CdSe QDs capped with L/D-

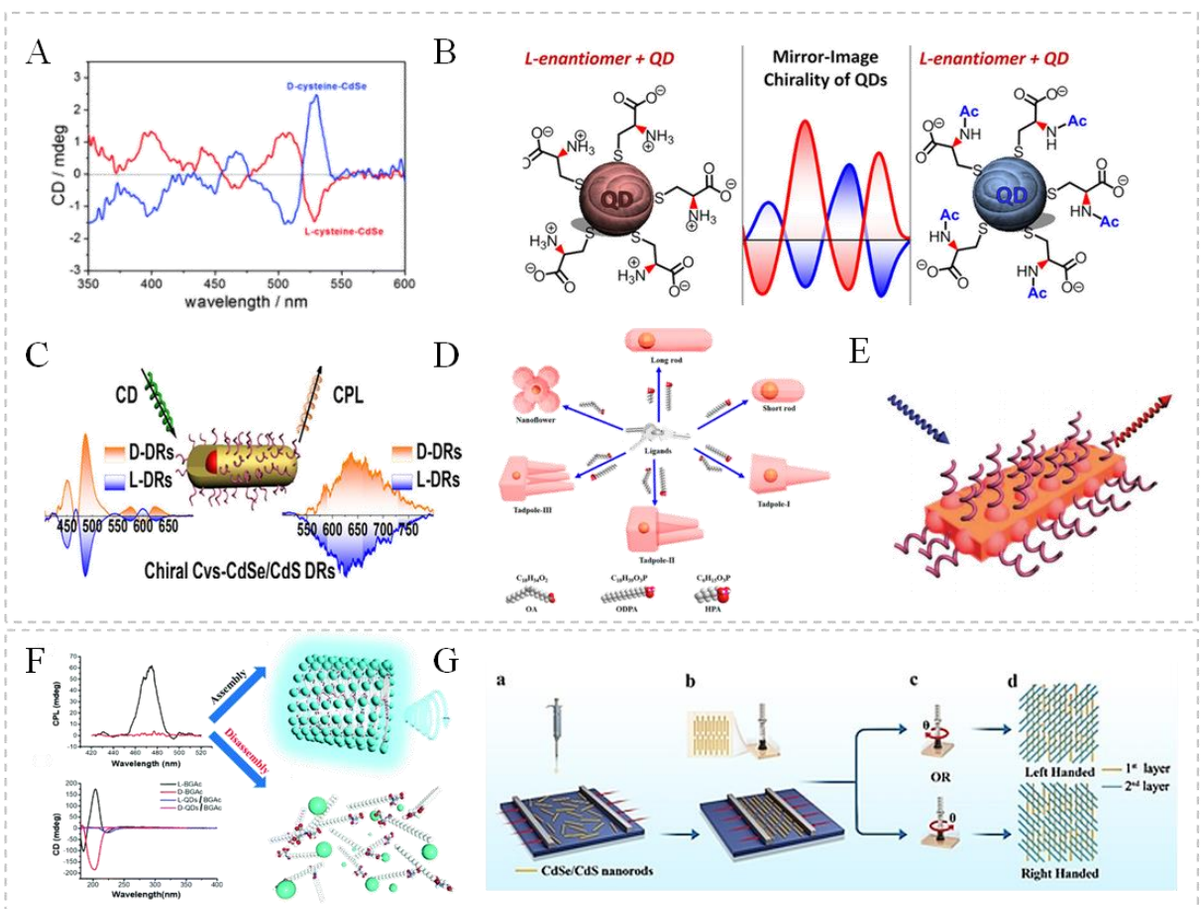

Figure 2 (A) CD spectra of L-Cys - CdSe QDs and D-Cys - CdSe QDs[42]. (reproduced from ref. 42 with permission from Royal Society of Chemistry). (B) Chiral inversion achieved by chiral molecules with distinct structures but identical L-configuration[44]. (reproduced from ref. 44 with permission from American Chemical Society). (C) Schematic diagram of chiral Cys- CdSe/CdS QDs signals[45]. (reproduced from ref. 45 with permission from American Chemical Society). (D) Mechanism of ligand-induced shape variations[46]. (reproduced from ref. 46 with permission from American Chemical Society). (E) Schematic diagram of NPLs chiral signals[47]. (reproduced from ref. 47 with permission from Wiley). (F) CPL spectra of cyan-emissive QD-doped co-gels in the state of assembly and disassembly[50]. (reproduced from ref. 50 with permission from Royal Society of Chemistry). (G) Fabrication procedure for the CdSe/CdS nanorod solution chiral films[53]. (reproduced from ref. 50 with permission from Wiley).

Cys exhibited mirror-image CPL signals with opposite handedness, representing the first example of ligand-induced CPL in semiconductor QDs. More importantly, time-dependent density functional theory (TDDFT) calculations based on a $(CdSe)_{13}$ nanocluster model reproduced qualitatively consistent mirrored CD spectra while keeping the geometry of the QDs core unchanged. This supported that the primary origin of induced chirality was the hybridization between the highest occupied molecular orbital (HOMO) of the chiral ligand and the valence electronic states of the QDs, rather than distortion of the crystal lattice caused by ligand adsorption. The presence of chiral ligands breaks the symmetry of excitonic states and induces coupling between electric and magnetic transition dipoles, resulting in enhanced dissymmetric optical responses. This work provided key evidence for understanding the electronic origin of ligand-induced chirality. Subsequent studies further deepened the understanding of chiroptical activity in semiconductor nanocrystals. For example, Balaz and colleague demonstrated that inversion of the CD signal could be achieved without changing the absolute configuration of the chiral ligand, simply by modifying the chemical structure of ligand[44]. This finding revealed that the chiroptical activity of quantum dots depends not only on the absolute stereochemistry of the ligand, but more critically on the binding configuration and spatial arrangement of ligands on the QD surface. (Figure 2B). Later, Cheng and Hao's group systematically revealed the influence of nanocrystal geometry on CD and CPL performance from multiple dimensions. In 2018, they successfully prepared L-/D-Cys capped CdSe-dot/CdS-rod heterostructures (DRs)[45], which exhibited tunable CD and CPL behavior with a maximum luminescence dissymmetry factor (g_{lum}) of 4.66×10^{-4} (Figure 2C). They also proposed that QDs with a thinner shell and larger core was more favorable for chirality induction. In 2020, the same team systematically investigated a series of complex morphologies ranging from spherical nanocrystals (0D) to nanorods (1D) and further to tadpole-like structures consisting of a 0D head and a 1D tail[46] (Figure 2D). Through *in situ* experiments, they clearly demonstrated that the CD signal mainly originated from the CdS shell (tail), whereas the CPL signal predominantly originated from the CdSe core, achieving separation of the origins of CD (shell) and CPL (core). Based on this, they established a structure – property relationship showing that a thinner shell favors stronger coupling between the core and chiral ligands, leading to enhanced CPL, while a longer tail with higher anisotropy is more beneficial for strengthening CD signals. This work clarified that the optimization pathways for CD and CPL are fundamentally different. In 2021, they further reported tunable CPL signals in two-dimensional CdSe/CdS chiral nanoplatelets (NPLs) capped with chiral ligands[47] (Figure 2E). They systematically revealed that during the evolution from discrete islands to complete shell coverage both CD and CPL signals first increased and then decreased, with the maximum response appearing at the island-like shell formation stage. This study further emphasized the critical role of shell growth mode and surface geometry in regulating chiroptical properties.

Chiral template assembly is also one of the important strategies for constructing chiral semiconductor quantum dots. Its core concept is to use molecules, supramolecular systems, or biomacromolecules with intrinsic chiral structures as templates to induce inorganic quantum dots to form chiral structures such as helices, twisted ribbons, or asymmetric polyhedra through electrostatic interactions, coordination, hydrogen bonding, or van der Waals forces[48, 49]. Compared with directly introducing chirality during nucleation and growth using chiral ligands, the template assembly method usually does not significantly disrupt the original crystal structure and luminescence properties of quantum dots, while enabling stronger CD and CPL signals. Therefore, it has attracted increasing attention in recent years. In particular, template systems such as DNA, cellulose nanocrystals (CNC), peptide molecules, and chiral liquid crystals have been widely used for constructing high-performance chiral luminescent systems because of their intrinsic helical structures and tunable

supramolecular assembly capability. For example, Duan's group employed a supramolecular co-assembly strategy to embed achiral QDs into chiral molecular gelators[50]. The quantum dots and gelators underwent co-gelation in the aqueous phase, inducing originally achiral quantum dots to exhibit strong CPL (Figure 2F). Subsequently, Liu *et al.* reported a gelator molecule that could spontaneously self-assemble into two-dimensional nanosheets and achieved precise regulation of CPL through simple chemical stimulation[51]. This hierarchical assembly structure not only exhibited unique morphology but also significantly enhanced the optical properties. In addition, quantum dots can also assemble into chiral superstructures through van der Waals forces and electrostatic adsorption. For example, during the assembly process of CdSe nanoplatelets, the stress induced by surface ligands caused the originally flat stacked belts to twist, forming chiral ribbons with regular helical structures[52]. The Langmuir - Schaeffer (LS) technique can also be used to align quantum dots directionally to induce chirality. Kuang *et al.* reported a method for preparing semiconductor nanorod chiral films with high CPL activity using the LS technique (Figure 2G)[53]. By precisely rotating the substrate angle during the transfer of each layer, they forced the nanorod layers to stack at specific angles, thereby constructing chiral films with helical structures on the macroscopic scale, with a maximum g_{lum} value of 0.0997.

A new approach based on water/oil interfacial mediation has recently been developed for the synthesis of chiral semiconductor nanomaterials. Cai *et al.* reported an interface-assisted, chiral ligand - metal ion coordination-mediated strategy for the synthesis of core - shell quantum dots, which was used to prepare chiral CdSe@ZnS quantum dots with significantly enhanced CPL performance[19]. It is well known that when water-soluble chiral ligands are directly introduced during nucleation and growth, the resulting QDs often suffer from weak fluorescence and broad emission spectra due to abundant surface defects. In contrast, post-synthetic ligand exchange usually weakens the chiroptical signals because the chiral ligands are mainly confined to the outer shell surface and have limited electronic coupling with the QDs core[39]. This interfacial strategy successfully combines the advantages of strong chiral induction from direct aqueous synthesis with the high photoluminescence quantum yield of post-synthetically modified core - shell quantum dots. As a result, the obtained QDs simultaneously exhibit narrow emission peaks, high brightness, strong CD signal, and intense CPL. Furthermore, theoretical calculations revealed that the CdSe@ZnS model constructed with the L-His - Zn^{2+} complex exhibited significant core - ligand orbital hybridization. In contrast, when L-His was directly coordinated or adsorbed onto the pre-formed CdSe@ZnS surface, the orbital hybridization was much weaker. This result provided strong electronic-structure-level evidence that the coordination-mediated growth strategy can effectively overcome the shell-shielding effect. Specifically, the chiral ligand deeply participates in the shell growth process through coordination complexes, thereby effectively bypassing the screening effect of the ZnS shell and enabling strong orbital hybridization between the QDs core and the ligand. As a result, both the absorption dissymmetry factor (g_{abs}) and g_{lum} reached the 10^{-2} level (Figure 3). This work provides a new strategy for simultaneously achieving high luminescence efficiency and strong chiroptical activity in chiral core - shell semiconductor quantum dots.

3.4 Opto- and Chemo- Applications

3.4.1 Chiral Recognition and Ion Detection

Chiral semiconductor QDs have attracted increasing attention in enantioselective recognition and biosensing owing to their unique combination of tunable fluorescence, strong chiroptical responses, and abundant surface coordination sites[54, 55]. Unlike conventional molecular probes, chiral QDs can serve as both optical reporters and stereoselective recognition units, enabling highly sensitive discrimination of biomolecular enantiomers through fluorescence, CD, CPL and electrochemiluminescence (ECL) responses. Molecular recognition is one of the most important phenomena in chemistry and biology[56]. A representative pioneering work was reported by Gun'

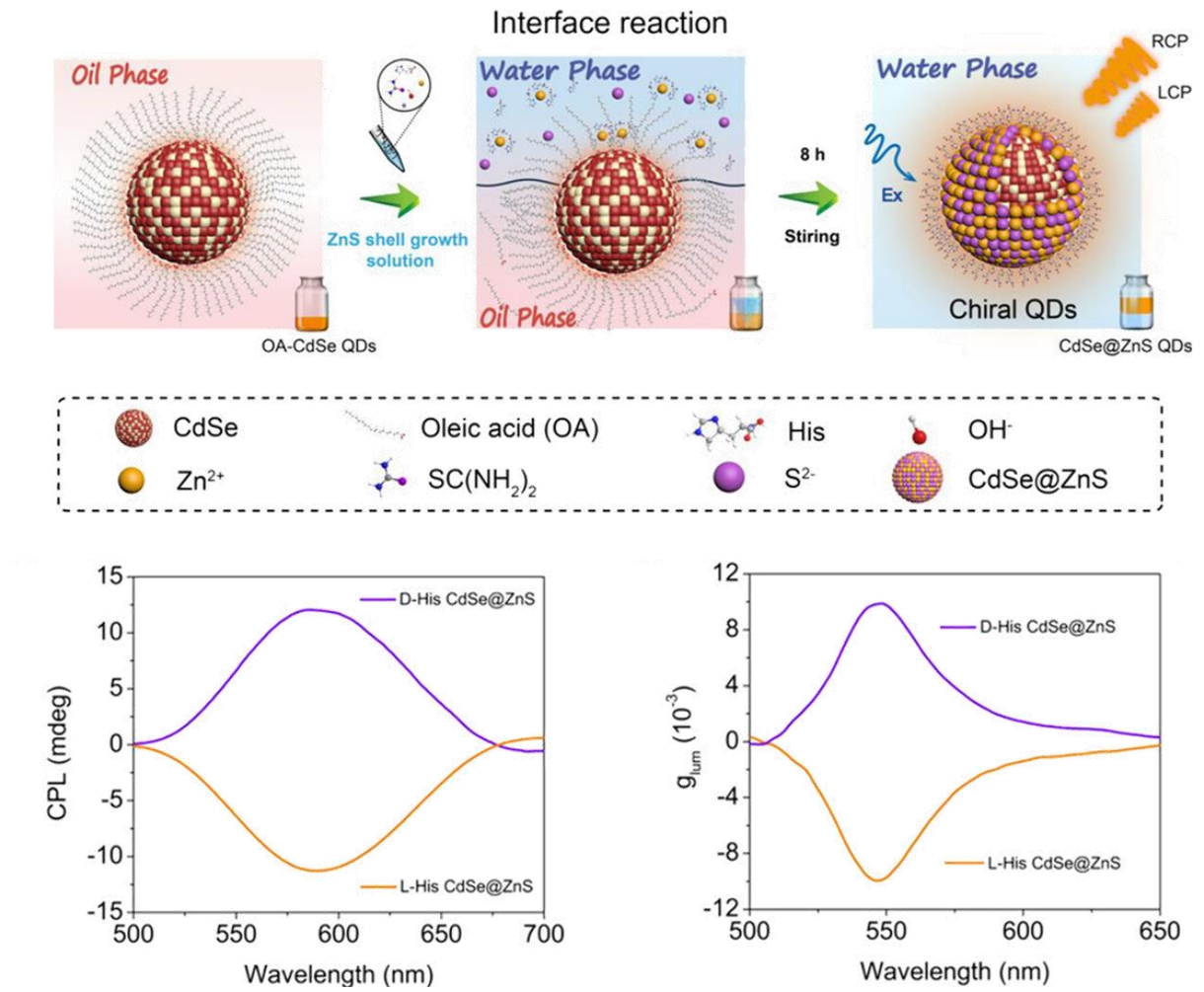

Figure 3 CdSe@ZnS at the oil – water interface achieves high luminescence dissymmetry factor and fluorescence quantum yield[19]. (reproduced from ref. 19 with permission from American Chemical Society).

ko and co-workers, who demonstrated that intrinsically chiral CdSe quantum dots could selectively recognize biomolecular enantiomers such as cysteine, histidine, and arginine[57]. They found that L-Cys preferentially adsorbed onto D-CdSe QDs, with up to 50-fold selectivity. This enantioselective interaction was confirmed by CD spectroscopy, real-time photoluminescence dynamics, and density functional theory calculations, providing direct evidence for stereoselective molecular recognition at the quantum dot surface. Subsequent studies further extended this concept to fluorescence sensing of amino acid enantiomers. For example, N-acetyl-L-cysteine-capped CdSe/CdS QDs were employed for the enantioselective recognition of tyrosine, originating from differences in surface binding affinity and hydrogen-bonding interactions[58].

Chiral semiconductor QDs, owing to their unique chiroptical activity, can also be employed for the detection of metal ions[59]. Compared with conventional fluorescence sensing, sensing strategies based on CD signals can effectively avoid spectral overlap and background fluorescence interference by monitoring the differential absorption of polarized light caused by the interaction between target analytes and the chiral microenvironment on the quantum dot surface[60]. The sensing mechanisms can generally be divided into two categories: signal quenching mode and signal generation mode. For example, Wang and co-workers developed a Pb^{2+} sensor based on chiral CdSe nanoplatelets[61]. In the presence of Pb^{2+} ions, the strong affinity between Pb^{2+} and the -SH of the chiral ligands disrupts the Cd – S bonds between the ligands and the nanoplatelet surface,

leading to ligand desorption. As a result, the chirality transfer pathway is interrupted, causing a significant decrease in the CD signal. Based on this principle, the sensor achieved a detection limit as low as 4.9 nM for Pb^{2+} and exhibited excellent selectivity among various coexisting ions due to the specific interaction between Pb^{2+} and -SH (Figure 4A). Time-dependent density functional theory (TD-DFT) calculations further revealed the mechanism of chirality generation and quenching at the electronic orbital level, providing theoretical guidance for sensor design. In contrast, Tedsana *et al.* employed chiral L-Cys capped CdS QDs for the detection of Ni^{2+} and Co^{2+}[62]. In this system, Ni^{2+} or Co^{2+} does not destroy the original chirality, instead, they coordinate with L-Cys on the quantum dot surface, forming in situ a new chiral metal complex with stronger optical activity. This newly formed structure generates distinct responses in the CD spectra: Ni^{2+} induces a negative CD signal at 324 nm, whereas Co^{2+} produces a positive CD signal at 352 nm (Figure 4B). Although the detection limits were at the micromolar level, the results obtained from real water samples were in good agreement with those measured by the standard method (ICP-OES), demonstrating the practical feasibility of this sensing strategy.

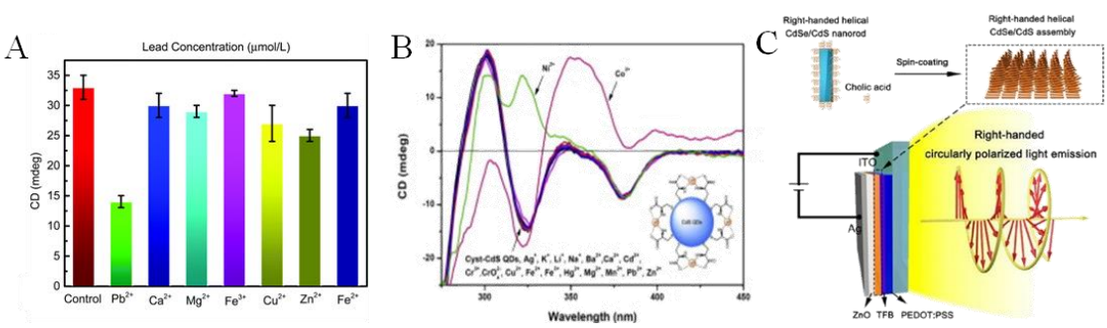

Figure 4 (A) Examination of the high selectivity of the CdSe NPL chiral sensor[61]. (reproduced from ref. 61 with permission from Royal Society of Chemistry). (B) CD spectrum of Cys-CdS QDs in the absence and presence of Ni^{2+} and Co^{2+}[62]. (reproduced from ref. 62 with permission from Elsevier). (C) Schematic diagram of chiral CdSe/CdS quantum rod-based light-emitting diodes[64]. (reproduced from ref. 64 with permission from Tsinghua University Press; Springer Nature).

3.4.2 Circularly Polarized Luminescence Devices

Among the various applications of chiral semiconductor QDs, circularly polarized light-emitting devices represent the most important and rapidly developing field. Unlike conventional luminescent devices, which require additional linear polarizers and quarter-wave plates to generate circularly polarized light, chiral quantum dots can directly emit CPL, thereby significantly simplifying device architecture and improving energy efficiency[63]. The first breakthrough was reported by Balaz and co-workers in 2013, who demonstrated ligand-induced CPL in CdSe quantum dots through post-synthetic ligand exchange using L-/D-Cys[43]. A major step toward practical applications was achieved in 2022, when chiral CdSe/CdS quantum rod-based light-emitting diodes were successfully fabricated to produce circularly polarized electroluminescence (CPEL)[64]. In this work, chiral CdSe/CdS QRs were synthesized with cholic acid as a symmetry-breaking agent, inducing a right-handed chiral dislocation. Remarkably, during spin-coating, these nanorods self-assembled into a long-range ordered helical superstructure with the helical axis perpendicular to the substrate. As shown in Figure 4C, this hierarchical chiral assembly not only served as the light-emitting layer but also functioned as an intrinsic circular Bragg reflector, selectively filtering the electroluminescence to produce a dominant right-handed CPEL signal at 600 nm. This evaporation-induced self-assembly strategy presents a feasible route for fabricating CPEL devices without complex templating. More recently, Cai and co-workers developed a coordination-mediated growth strategy at the liquid/liquid interface to prepare chiral CdSe@ZnS core – shell quantum dots with significantly enhanced CPL performance[19]. By introducing chiral His – Zn^{2+} complexes during shell growth, the resulting quantum dots achieved both high photoluminescence quantum yield

and exceptionally large glum values at the 10^{-2} level. This work provides an effective strategy for overcoming the long-standing trade-off between strong luminescence efficiency and strong chiroptical activity, greatly advancing the development of high-performance CPL-emitting devices.

3.4.3 Spintronic Devices and Emerging Applications

In addition to light emission, the chiral-induced spin selectivity (CISS) effect in chiral semiconductors enables the realization of emerging spintronic optoelectronic devices. Current studies have shown that electron transport through chiral molecules depends on the electron spin orientation, a phenomenon known as the CISS effect[65]. A pioneering study demonstrated that simple chiral molecules adsorbed on metal surfaces can induce magnetization switching of the underlying ferromagnetic (FM) thin film without the need for an external current or magnetic field. This result provided direct evidence for light- or electron-induced local magnetization in the absence of an external magnetic field, offering a theoretical foundation for constructing highly spin-polarized nanoscale devices[66]. The integration of chiral semiconductor QDs into solid-state devices represents a transition toward magnet-free spintronics. Bloom and co-workers demonstrated that thin films of CdSe QDs capped with L-/D-Cys can act as efficient spin filters at room temperature via the CISS effect[67]. In magnetic conducting atomic force microscopy (mCP-AFM) measurements, these chiral quantum dot films exhibited a pronounced dependence of tunneling current on the magnetization direction of the tip, corresponding to an effective spin-dependent barrier height difference of approximately 0.2 eV. This spin filtering behavior was further confirmed in magnetoresistance devices. Notably, the effect was quenched in larger (6 nm) quantum dots, highlighting that spin selectivity originates from the chiral imprinting of ligand-induced electronic states under strong quantum confinement[65].

Furthermore, the unique combination of high quantum yield and tunable CPL signals makes chiral QDs ideal candidates for anti-counterfeiting and information encryption. Integration of chiral QDs into polymer matrices or via inkjet printing enables the fabrication of flexible, high-resolution security tags and wearable 3D imaging systems.

4 Chiral carbon quantum dots

4.1 One-Pot Synthetic Method

Compared with traditional semiconductor QDs containing toxic heavy metals such as cadmium and lead, CQDs exhibit lower toxicity, superior biocompatibility, lower cost, and facile surface functionalization[68]. These advantages endow CQDs have attracted increasing attention in recent years with significant potential for biological applications, including bioimaging, biosensing, and drug delivery[68-71]. In 2016, Kang and co-workers reported the first example of intrinsically chiral carbon quantum dots[17]. As shown in Figure 5A, using a one-pot synthetic strategy, a chiral precursor was directly involved in the formation of the carbon core. Notably, the chiral configuration of the precursor was retained during the carbonization and polymerization processes and became embedded within the carbon core framework, rather than being merely adsorbed on the surface. This work realized the direct transfer of chirality from the molecular level to the nanoscale. The CD spectra of L-CQDs and D-CQDs exhibit perfect mirror-image Cotton effects at 245 and 350 nm, confirming the successful construction of intrinsic chirality at the nanoscale. Prior to this study, research on CQDs mainly focused on their photoluminescence properties, while systematic investigations of chiral CQDs were scarce and largely limited to conceptual demonstrations or complex post-modification strategies. In addition, Kang and co-workers were the first to apply chiral CQDs for enantioselective recognition. In 2018, Kang's group further developed this strategy by employing a one-step hydrothermal method using citric acid and chiral cysteine as precursors, achieving efficient chirality transfer from molecules to nanomaterials[72]. The obtained L- and D-CQDs exhibited mirror-image CD signals at approximately 212 and 250 nm, along with high photoluminescence quantum yields (~30%) and excellent pH and thermal stability. More importantly, they discov-

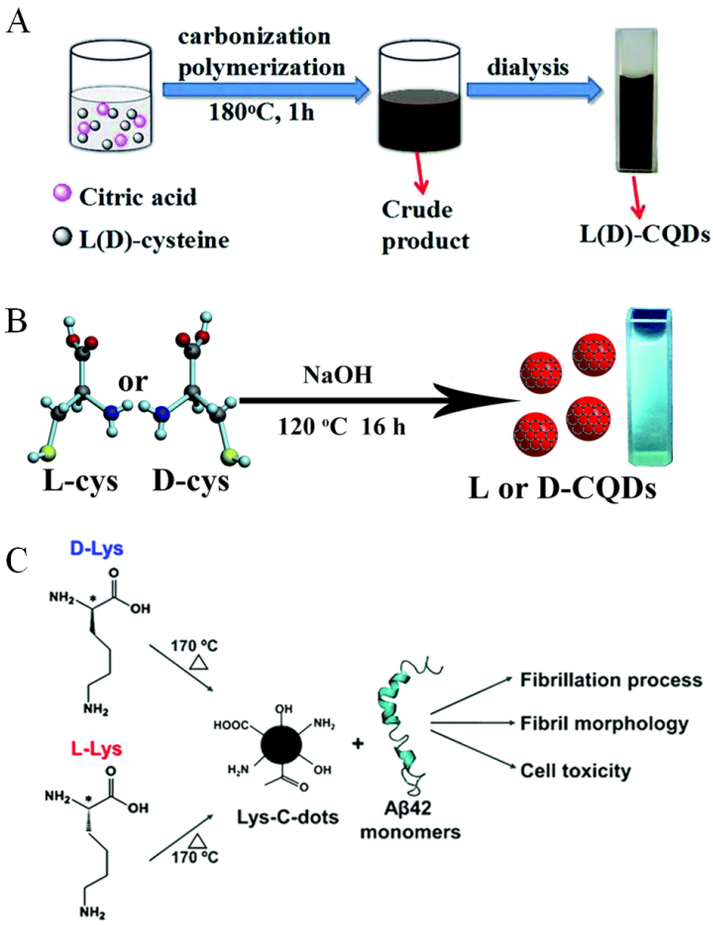

Figure 5 (A) Synthesis strategy of L-CQDs and D-CQDs[17]. (reproduced from ref. 17 with permission from Royal Society of Chemistry). (B) Schematic for the synthesis of L- or D-CQDs[73]. (reproduced from ref. 73 with permission from Royal Society of Chemistry). (C) Synthesis scheme of chiral CQDs[74]. (reproduced from ref. 74 with permission from Royal Society of Chemistry).

ered that D-CDs significantly outperform L-CDs in promoting root activity, Rubisco enzyme activity, and photosynthesis efficiency, with enhancement factors ranging from 20% to 67%. This work represents the first systematic demonstration of stereoselective growth regulation in plants induced by chiral CQDs.

Chiral amino acids, which inherently contain carbon elements, can simultaneously serve as both carbon sources and chirality inducers during CQD synthesis. For example, in 2017, Kang's group reported the one-step synthesis of nitrogen- and sulfur-co-doped chiral CQDs (L-/D-CQDs) using a single chiral precursor L-/D-Cys (Figure 5B)[73]. The resulting CQDs exhibited strong mirror-symmetric CD signals at approximately 212 and 240 nm. This strategy avoids the structural uncertainty associated with mixed precursor systems. Importantly, they proposed an insightful concept that photoluminescence (PL) and CD are fundamentally independent properties. With increasing temperature, the fluorescence intensity gradually decreases due to thermal quenching (with a linearity of 0.992), whereas the CD signal remains nearly unchanged. This finding challenges the earlier assumption that chirality necessarily influences luminescence and provides a crucial theoretical basis for the design of multifunctional chiral nanomaterials. In 2018, Raz Jelinek and co-workers reported another significant advance by synthesizing chiral CQDs using a single chiral precursor L- or D-lysine as the sole carbon source (Figure 5C)[74]. These CQDs demonstrated enantioselective inhibition of amyloid fibrillation, a key pathological process in Alzheimer's disease. Experimental results showed that L-CQDs exhibit significantly higher inhibitory efficiency toward

Aβ42 aggregation and provide better neuroprotection compared to their D-counterparts. This behavior can be attributed to the specific stereochemical matching between the surface functional groups of L-CQDs and Aβ42 peptides.

4.2 Two-Step Synthesis Method

The two-step strategy is an important approach for the preparation of CQDs, in which achiral carbon cores are first generated through carbonization of precursors, followed by surface modification with chiral molecules to impart chirality to the final products. Unlike the one-step hydrothermal method, where chiral precursors are directly carbonized, the two-step strategy typically involves the initial synthesis of carbon dot cores with excellent luminescent properties, followed by post-synthetic functionalization to introduce chiral centers. This process not only enables surface passivation but also creates new emissive centers, thereby enhancing fluorescence intensity. More importantly, this method preserves the structural integrity of the chiral ligands, allowing the final products to fully inherit the optical characteristics of the chiral sources.

Early studies commonly employed citric acid or glucose as carbon sources to prepare highly fluorescent carbon dots via hydrothermal synthesis, followed by surface modification using chiral molecules such as L-/D-Cys, Pen and proline. Such post-modification strategies can achieve stable chirality transfer through covalent bonding or coordination interactions between the ligands and the surface carboxyl, hydroxyl, and amino groups of carbon dots, while significantly enhancing CD and CPL signals. Among them, the cysteine system has become one of the most widely used chiral sources because it contains both thiol and amino groups, which enable stronger interactions with the carbon dot surface[75]. For example, Suzuki *et al.* first prepared achiral graphene QDs precursors with sizes of 2 – 7 nm and carboxyl-rich edges (– COOH) through a top-down acid oxidation exfoliation method, such as treating carbon fibers with a mixed sulfuric acid/nitric acid solution[76]. Subsequently, at room temperature, L-/D-Cys molecules were covalently attached to the edge carboxyl groups of achiral QDs through an amidation reaction using 1-ethyl- (3-dimethylaminopropyl) carbodiimide (EDC) and N-hydroxysuccinimide (NHS) as coupling agents (Fig. 6A). New CD signals were

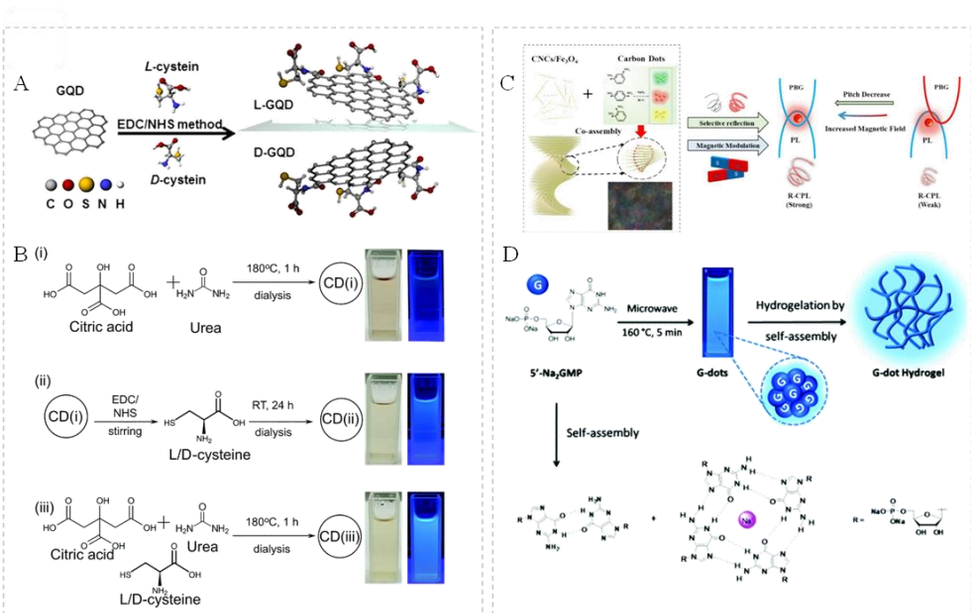

Figure 6 (A) Schematic diagram of two-step synthesis of CQDs[76]. (reproduced from ref. 76 with permission from American Chemical Society). (B) Scheme of the syntheses of CD(i), L/D-CD(ii) and L/D-CD(iii)[77]. (reproduced from ref. 77 with permission from Royal Society of Chemistry). (C) Schematic diagram of CQDs synthesis via self-assembly of CNC templates[79]. (reproduced from ref. 79 with permission from Elsevier). (D) Formation of 5′-GMP CQDs[80]. (reproduced from ref. 80 with permission from Royal Society of Chemistry).

observed at approximately 250 – 265 nm, corresponding to the excitonic absorption of GQDs rather than the molecular absorption of cysteine. This result indicated that chirality was not merely confined to the surface but was transferred to the electronic energy levels of the entire carbon core. Combined with DFT and molecular mechanics calculations, they further revealed that this distortion effect exhibited strong size dependence: only small-sized GQDs (2 – 7 nm) could maintain stable twisted conformations. As shown in Fig. 6B, Rogach *et al.* systematically compared two chiral carbon dot synthesis strategies based on L-/D-Cys[77]. They found that both methods significantly improved the PLQY, whereas the surface-modified carbon dots exhibited much stronger chiral signals than those prepared by direct carbonization of chiral precursors.

In addition, the two-step strategy has been widely used for constructing functional composite systems. For example, Lin and co-workers proposed an organic – inorganic co-assembly strategy, successfully inducing the assembly of achiral CQDs into nanospiral structures with strong CPL activity[78]. Through interfacial kinetic regulation, they achieved the synergistic amplification of chiral signals and emission polarization, increasing the CPL dissymmetry factor of CPDs to the 10^{-2} level. Xu and co-workers further constructed composite nanomaterials with chiral recognition capability and tunable chiroptical properties by co-assembling achiral CQDs, magnetic Fe_3O_4 nanoparticles, and chiral templates (Figure 6C)[79]. Such strategies have greatly expanded the applications of chiral carbon dots in bioimaging, sensing, and intelligent chiral optoelectronic devices. Ghosh *et al.* reported the direct synthesis of chiral carbon dots using naturally occurring guanosine-5′-monophosphate (5′-GMP) as the sole precursor[80]. Since guanine groups remained on the surface of the G-dots, they could further self-assemble to form chiral supramolecular hydrogels (Figure 6D).

4.2 CPL-related Applications

CQDs have attracted considerable attention in recent years as emerging chiroptical nanomaterials for CPL sensors and optical information devices. Their ability to generate CD and CPL signals enables them to serve not only as conventional fluorescent emitters but also as advanced polarization-sensitive optical materials[81]. In particular, the combination of strong fluorescence and chiral optical responses provides a new platform for high-sensitivity sensing, multi-level information encryption, anti-counterfeiting, and intelligent photonic devices. Among these applications, CPL-based sensing has become one of the most important research directions. Unlike conventional fluorescence sensing, which mainly relies on intensity variation and is often affected by background fluorescence and spectral overlap, CPL sensing uses the difference between LCPL and RCPL as the output signal, significantly improving selectivity and anti-interference capability. Because the CPL response is highly sensitive to changes in the local chiral environment, small perturbations caused by ions, biomolecules, or structural transformations can induce remarkable variations in the g_{lum}, thereby enabling highly sensitive detection. Wang and co-workers recently developed a novel CPL sensor for the dual detection of Hg^{2+} and I^- based on G-quartet nanofibers and N/S co-doped achiral CQDs[82]. In this system, the G-quartet-based nanofibers (g-fibers), formed by guanosine 5′-monophosphate (GMP) units linked through hydrogen bonding, served as chiral templates to transfer chirality to the achiral carbon dots and induce strong CPL signals. The resulting luminescence dissymmetry factor (g_{lum}) reached the 10^{-2} level. More importantly, the obtained chiral composites were successfully applied to the dual detection of Hg^{2+} and I^- ions using CPL as the signal output. The detection limit for Hg^{2+} was 88.4 nM, while that for I^- was 157 nM. (Figure 7A). In addition, Zhang and co-workers found that CQDs, synthesized using L-tryptophan and D-tryptophan as precursors, could trigger the supramolecular self-assembly of N-(9-fluorenylmethoxycarbonyl)-protected glutamic acid (Fmoc-Glu), forming chiral hydrogels with left-handed or right-handed helical nanostructures[83]. This material exhibited strong chiral templating capability and enabled universal chirali-

ty transfer to embedded dye molecules, thereby achieving full-color CPL and Förster resonance energy transfer (FRET) -based CPL. Furthermore, transparent composite films prepared by combining the chiral hydrogels with poly(vinyl alcohol) (PVA) exhibited differential responses toward LCPL and RCPL (RCP). These films could therefore serve as simple and visual circularly polarized light detectors or optical polarization filters for distinguishing LCPL from RCPL (Figure 7B). Importantly, chiral carbon dots are also highly suitable for secure optical storage and anti-counterfeiting labels. Li *et al.* synthesized four types of chiral carbon dots with emissions ranging from near-ultraviolet to red light and co-assembled them with cellulose nanocrystals (CNCs) to fabricate a series of C QDs@CNCs composite films[84]. Owing to the left-handed chiral nematic structure of CNCs and the tunable fluorescence of CCDs, these films exhibited distinct visual polarization differences under circular polarizers with different rotation directions (Figure 7C). This provides significant opportunities for the application of CPL materials in information encryption, optical anti-counterfeiting, and polarization detection.

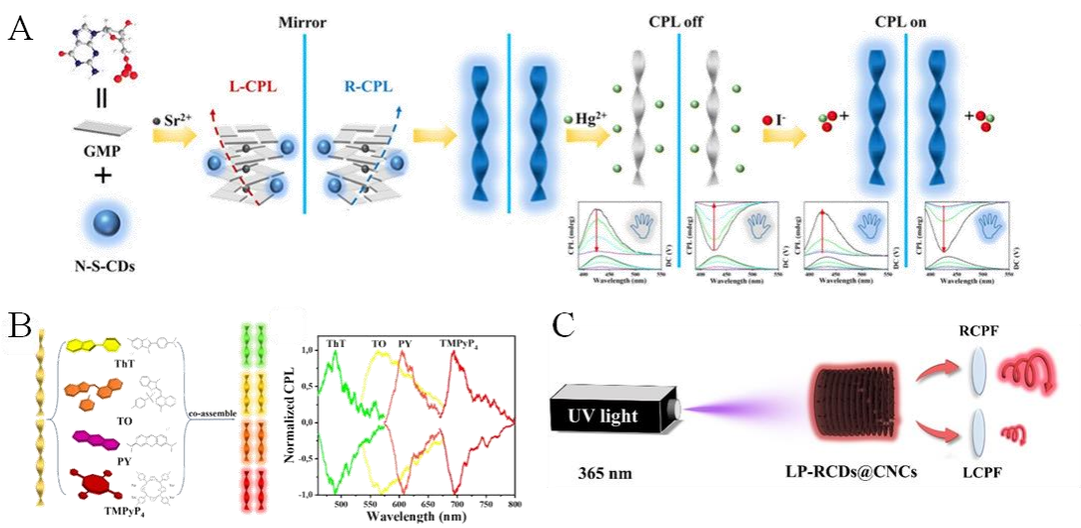

Figure 7 (A) Schematic illustration of the CPL sensor constructed by the co-assembly of the left-handed and right-handed N - S-CDs/g-fiber[82]. (reproduced from ref. 82 with permission from Royal Society of Chemistry). (B) Schematic illustration of co-assembly between four typical dye molecules and hydrogels template[83]. (reproduced from ref. 83 with permission from Elsevier). (C) Schematic diagram of the LP-RCDs@CNC composite film for visual polarization detection[84]. (reproduced from ref. 84 with permission from Elsevier).

5 Chiral Perovskites

In recent years, chiral perovskites have attracted extensive attention owing to their unique applications in CPL, spintronics, and optoelectronic photodetection. The fundamental principle lies in breaking the spatial inversion symmetry of the crystal structure through the introduction of chiral motifs, thereby endowing the material with chiroptical responses. Compared with inorganic QDs, one remarkable advantage of perovskite materials is their highly tunable crystal structure and bandgap, which can be flexibly adjusted by engineering the organic and inorganic structural units. Therefore, the rational introduction of functional organic cations provides an effective strategy for constructing novel perovskite architectures with tailored chiroptical and optoelectronic properties. In 2003, David G. Billing and coworkers first reported the single-crystal structure of the chiral organic - inorganic hybrid perovskite (S)-PEA·$PbBr_3$, marking the earliest example of chiral hybrid perovskites[85]. This pioneering work initiated systematic investigations into the crystal structures of a wide range of chiral halide perovskites[86-90]. Following the above classification, the synthetic strategies of chiral perovskites can be generally classified into three major categories: (i) direct construction via

the introduction of chiral organic cations, (ii) post-synthetic modification through surface engineering with chiral ligands, and chirality induction through supramolecular or physical assembly.

5.1 Direct Construction Strategy

Direct incorporation of chiral organic cations is one of the most mature crystal growth strategies for preparing chiral perovskite nanocrystals. In this approach, chiral ammonium salts are introduced during precursor preparation, allowing chiral cations to participate directly in crystal growth through covalent and ionic interactions, thereby inducing chirality within the perovskite lattice itself. This method enables precise control over the size, shape, and dimensionality of hybrid organic – inorganic perovskites (HOIPs) through rational precursor substitution and structural design. In 2006, David G. Billing systematically reported a series of chiral two-dimensional layered perovskites, such as $(PEA)_2PbI_4$[91]. By employing chiral organic amines as structure directing agents and using slow solution crystallization, they achieved controllable synthesis of chiral hybrid materials ranging from 1D to 2D architectures. This work filled the gap of chiral hybrid materials in the perovskite field and laid the structural foundation for subsequent studies extending from single crystals to thin films, nanosheets, and QDs. For example, in 2018, Waldeck and co-workers reported the direct synthesis of chiral methylammonium lead bromide perovskite nanoplatelets using R- or S-phenylethylammonium (PEA) ligands combined with achiral OA ligands[18]. Distinct bisignate Cotton effects were observed at the excitonic absorption region from 400 nm to 450 nm, demonstrating the successful transfer of chirality to the band-edge electronic states of the inorganic core. Their study showed that the CD signals originated from the chiral imprinting of surface ligands on the electronic states of the nanoplatelets rather than from aggregation effects. Subsequently, Xu synthesized two-dimensional perovskite nanowires with a non-centrosymmetric crystal structure via a one-step approach and realized strong second-harmonic generation (SHG) together with chiral nonlinear optical responses[92]. In this system, R/S-MPEABr served as the structure-directing agent, where the chiral center directly disrupted inversion symmetry within the crystal lattice. In addition, Gao *et al.* reported 3D hybrid organic – inorganic perovskites that implant chirality through introducing the chiral methylammonium cation are demonstrated Figure 8A[93].

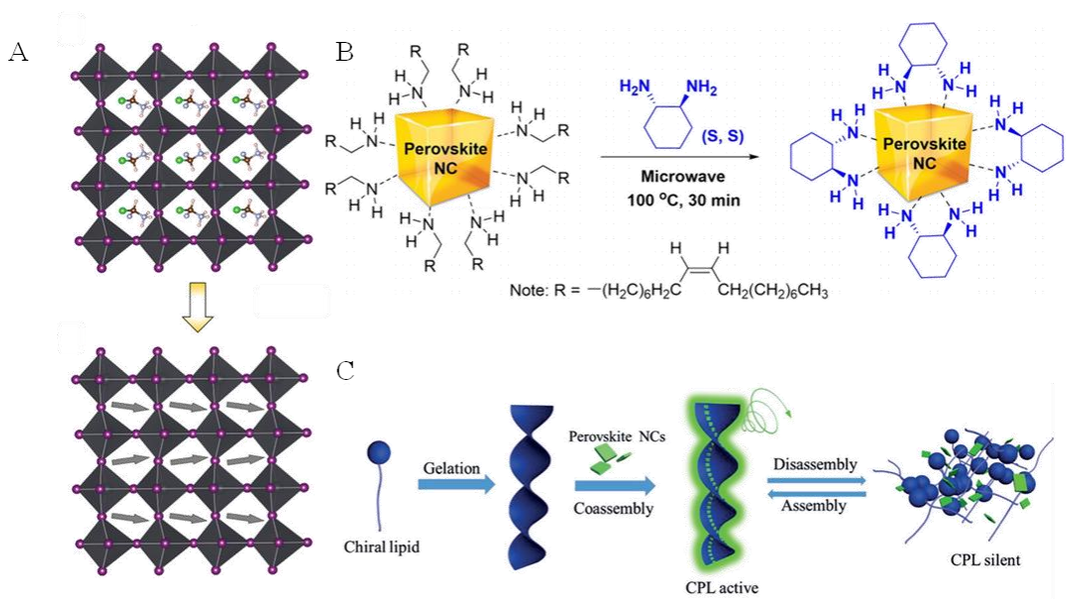

Figure 8 (A) The structures of 3D chiral HOIPs (R)-$CHFClNH3PbI_3$[93]. (reproduced from ref. 93 with permission from Wiley). (B) Ligand exchange on an OA-capped perovskite NC using enantiomers[94]. (reproduced from ref. 94 with permission from AIP Publishing). (C) Schematic diagram of the co-assembly induced chirality of perovskite NCs in chiral gels[95]. (reproduced from ref. 95 with permission from Wiley).

5.2 Post-Synthetic Modification and Assembly Strategy

In post-synthetic modification, achiral perovskite nanocrystals are first prepared, followed by ligand exchange reactions in which external chiral molecules partially or completely replace the original surface ligands. Chirality is then transferred from the ligands to the perovskite core, generating chiroptical activity. In such systems, chirality mainly originates from the formation of non-centrosymmetric surface structures and chiral spatial arrangements induced by surface ligands. The mechanism is often more complex and strongly dependent on ligand concentration. In 2017, Zhang synthesized chiral all-inorganic perovskite nanocrystals by grafting chiral molecules onto the surface of achiral nanocrystals through microwave-assisted ligand exchange[94], as shown in Figure 8B. These materials possess unique advantages such as long carrier lifetimes and high luminescence efficiency. They found that the origin of chirality strongly depended on the amount of the chiral ligand. When excessive ligand was used, chirality mainly originated from chiral pattern aggregation of ligands on the nanocrystal surface. In contrast, under low ligand concentration, chirality primarily arose from ligand-induced surface lattice distortion, defect formation, and electronic interactions. Interestingly, even after removing the ligands, part of the CD signal remained, directly proving that surface distortion serves as the physical basis for chirality retention.

Chiral assembly has also emerged as an effective route for obtaining highly luminescent chiral perovskites. For example, Liu *et al.* realized CPL indirectly by supramolecular co-assembly on the macroscopic scale[95], where achiral perovskite nanocrystals borrowed optical activity from an external chiral gel network shown in Figure 8C. In this system, chirality was transferred through a chiral field and spatial confinement rather than through strong chemical bonding. Furthermore, the co-gel was directly embedded into a PMMA matrix to fabricate self-supporting flexible CPL films, demonstrating promising device applications. Similarly, Wang and co-workers achieved high-performance CPL by physically integrating achiral perovskite emitters with chiral liquid crystal (CLC) filters[96]. They proposed a separation of emission and chirality concept, in which efficient and stable achiral perovskites are responsible for light emission, while chirality is provided by specialized CLC filters. In addition, Ma *et al.* confirmed that the generation of chirality in chiral perovskites $(R\text{-/S-MBA})_2PbI_4(1-x)Br_4x$ is mainly attributed to the electronic interactions between the chiral organic spacer cations and the inorganic framework[97]. They found that the microstrain induced by spatial confinement leads to the redistribution of the stacking conformation of the benzene rings in the organic spacer cations, which enhances the asymmetric hydrogen-bonding interactions between the chiral organic molecules and the inorganic framework. This asymmetry promotes the transfer of chirality from the organic molecules to the inorganic framework. More recently, Liu *et al.* reported a new strategy for preparing strongly circularly polarized red-emissive perovskite nanowires through chiral ligand-induced self-assembly[98]. The obtained chiral $CsPbI_3$ nanowires exhibited intense circularly polarized red emission at ~640 nm, with a film-state luminescence dissymmetry factor. This work effectively addressed several long-standing challenges in chiral perovskites, particularly in the red and near-infrared regions, including low g-factors, poor stability, and harsh synthetic conditions.

5.3 Optoelectronic Applications

Chiral perovskites have emerged as one of the most promising material systems for direct CPL detection because they combine the polarization-selective absorption of chiral organic molecules with the excellent charge transport properties of inorganic perovskite frameworks. Unlike conventional CPL photodetectors, which require additional optical components such as quarter-wave plates and linear polarizers, chiral perovskites can directly distinguish LCPL from RCPL, thereby significantly simplifying device architecture and enabling highly integrated optoelectronic systems[99-103].

Ahn *et al.* observed a pronounced Cotton effect

in phase-pure two-dimensional perovskite thin films containing chiral organic cations. The R- and S-type films exhibited CD signals with opposite signs. In addition, the CD response could be tuned by controlling the morphology, thickness, and orientation of the films. This novel finding demonstrated that chiral perovskites possess differential absorption toward LCPL AND RCPL, which provides the physical foundation for constructing CPL photodetectors[87]. A pioneering breakthrough was reported by Chen *et al.* in 2019, who first demonstrated a high-performance direct CPL photodetector based on the chiral hybrid perovskite[88]. The device achieved a high responsivity of 797 mA W^{-1}, a detectivity of 7.1×10^{11} Jones, and a 3-dB bandwidth of 150 Hz, while maintaining excellent operational stability for over one month (Figure 9A) Flexible devices fabricated on PET substrates also showed comparable performance, highlighting the strong potential of chiral perovskites for wearable CPL-sensitive electronics. Subsequent studies further expanded CPL photodetection toward multifunctional intelligent devices. For example, Liu *et al.* constructed a circular polarization-resolved ultraviolet photonic artificial synapse by integrating helical chiral perovskites with single-wall carbon nanotubes[104]. This work extended CPL detection from conventional photodetection to neuromorphic vision systems. More recently, panchromatic CPL detection was achieved through 3D/chiral-2D perovskite heterostructures[105].

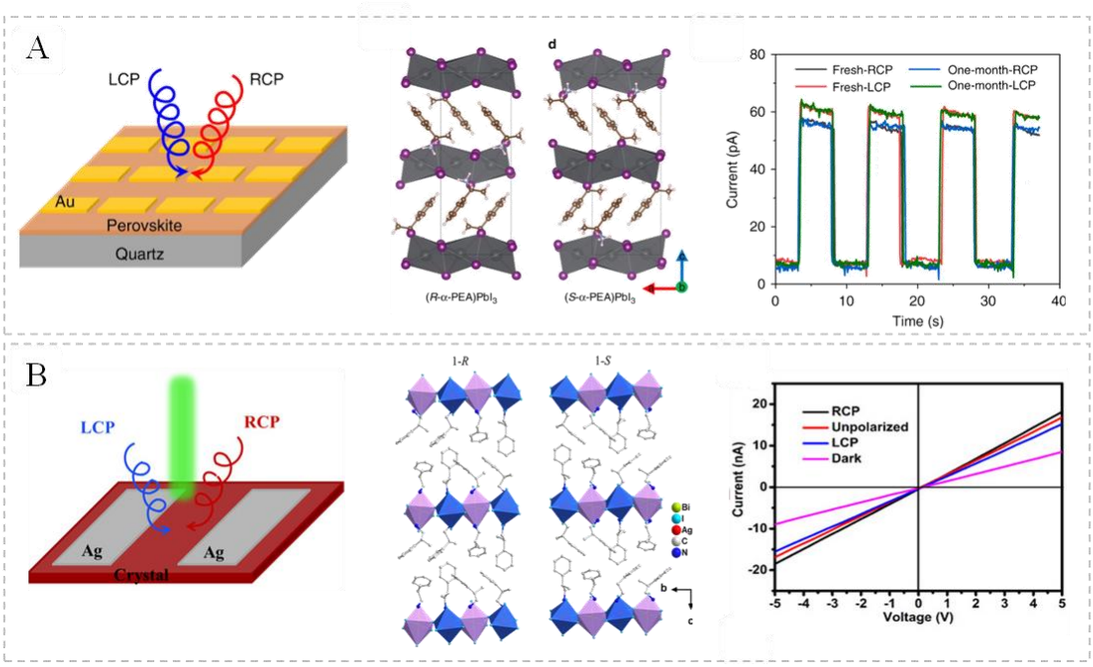

Figure 9 (A) Schematic diagram of photodetector; The crystal structure of (R- and S-α-PEA)PbI_3; Photoresponse of fresh and 1-month aged (S-α-PEA)PbI_3 films under LCP and RCP 395 nm light[88]. (reproduced from ref. 88 with permission from Springer Nature). (B) Schematic diagram of CPL photodetector; Layered structure viewed along a axis; The current - voltage curves of device under dark, LCP-520, RCP-520, and unpolarized-520 nm light illumination[107]. (reproduced from ref. 107 with permission from Wiley).

In contrast, lead-free chiral perovskites have attracted increasing attention because of concerns regarding Pb toxicity. Li *et al.* developed the lead-free double perovskite and achieved the first self-powered CPL photodetector without any external power supply[106, 107]. Benefiting from the chiral polar photovoltaic effect, the device showed an anisotropy factor as high as 0.3, representing one of the best performances among lead-free chiral perovskite detectors (Figure 9B). This work demonstrates that environmentally friendly lead-free perovskites can serve as highly competitive candidates for next-generation green CPL photodetectors.

In addition, chiral perovskites have been ex-

plored for applications in light-emitting diodes (LEDs) due to their advantages of high photoluminescence quantum yield, narrow emission bandwidth, and tunable bandgap. More importantly, chiral perovskites can induce spin-selective effects, making them efficient spin filters in spin-polarized LEDs. Current chiral perovskite LED strategies are mainly divided into two categories: spin-filter-assisted LEDs and intrinsically emissive LEDs. In the first strategy, chiral perovskites serve as spin-filtering layers that selectively transport spin-polarized carriers, while the emissive layer remains achiral. This approach effectively utilizes the CISS effect to generate CPEL without external magnetic fields or ferromagnetic electrodes. Beard's group first used chiral two-dimensional perovskite (R-/S-MBA)$_2$PbI$_4$ as the CISS layer to directly generate CPL inside the device[106]. The device exhibited a spin-polarized hole current exceeding 80%, and its spin orientation was determined by the chirality of the MBA cations, as shown in Fig. 10A. In the second strategy, the chiral perovskite itself functions as both the emissive layer and the spin-selective medium, allowing the direct generation of CPL through radiative recombina-

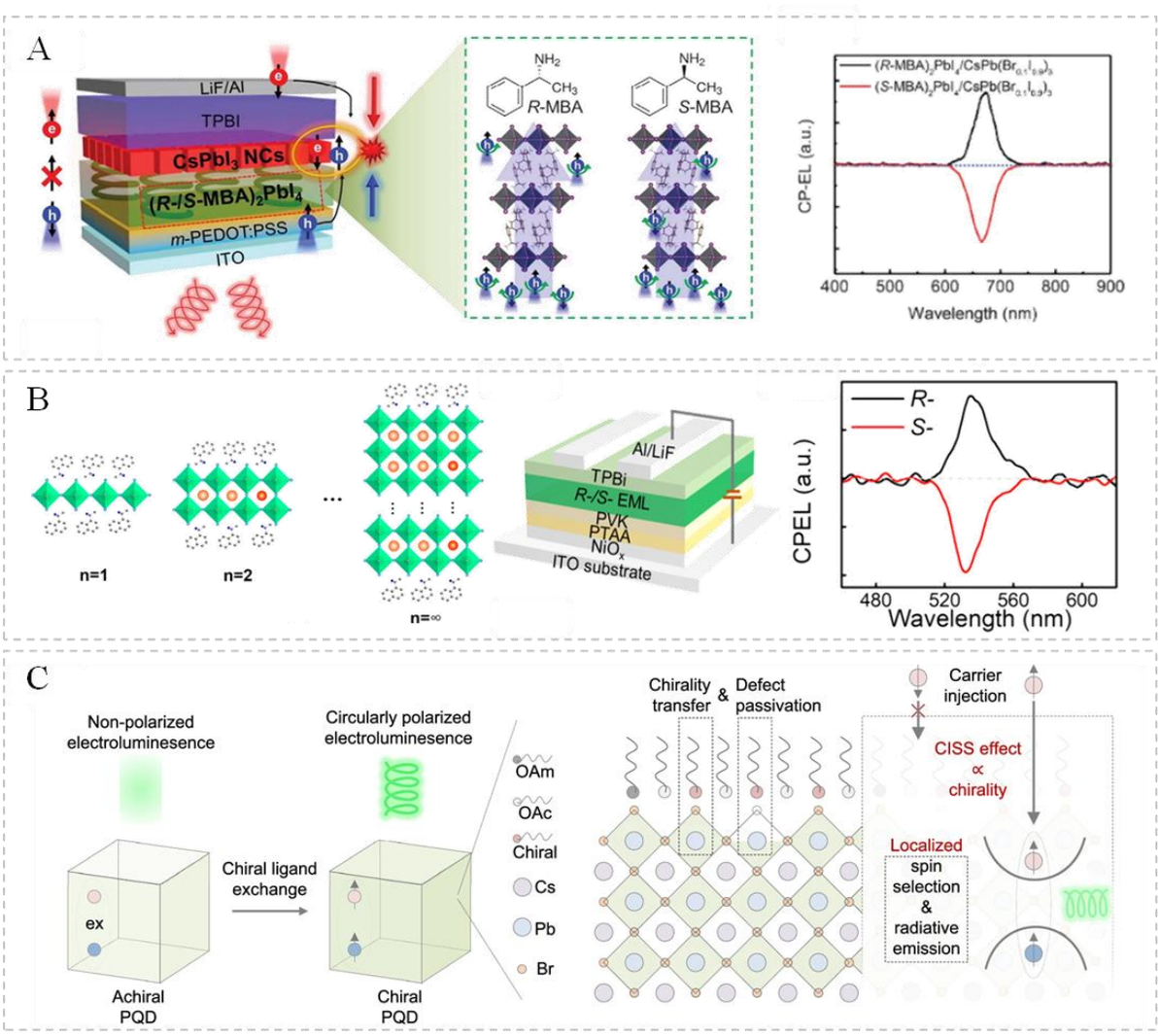

Figure 10 (A) Schematic of spin-polarized charge injection and CP-EL emission; CPEL of spin-LEDs based on CISS layer/$CsPbBr_3$[106]. (reproduced from ref. 106 with permission from American Association for the Advancement of Science). (B) Schematic illustration of quasi-2D perovskites; Structure and EL performance of spin-LEDs; CPEL spectra of spin-LEDs[108]. (reproduced from ref. 108 with permission from American Chemical Society). (C) Schematic illustration of the mechanism of spin-LEDs based on chiral PQDs[109]. (reproduced from ref. 109with permission from Springer Nature).

tion. For example, Yao *et al.* reported highly efficient green spin LEDs based on quasi-two-dimensional chiral perovskites, in which the chiral perovskite served as the emissive layer to achieve efficient CPEL, with a photoluminescence quantum yield of 91%, a g_{lum} of 8.6×10^{-2}, an electroluminescence dissymmetry factor (g_{EL}) of 7.8×10^{-2}, and a maximum external quantum efficiency (EQE) of 13.5%, as shown in Fig. 10B106[108]. This strategy does not require an additional spin-filtering layer and enables spin regulation through a single chiral emissive layer, thereby reducing device complexity.

At present, both the EQE and CPEL of chiral perovskite-based spin LEDs remain relatively low. Recently, Song *et al.* reported spin light-emitting diodes based on chiral perovskite quantum dots, achieving both high circular polarization and high efficiency[109]. By improving the efficiency of chiral ligand exchange and spin selectivity, these devices exhibited remarkable electroluminescence dissymmetry factors of 0.285 (R) and 0.251 (S), together with high EQEs of 16.8% and 16.0%, respectively (Fig. 10C). High g_{EL} values are often obtained at the expense of luminescence efficiency, whereas this work successfully achieved both simultaneously, greatly enhancing the practical potential of chiral perovskite LEDs.

4 Conclusion and perspectives

In summary, CPL-active inorganic quantum dots have developed into one of the most important research directions in chiral nanomaterials due to their unique combination of strong luminescence, tunable electronic structures, and controllable chiroptical responses. Compared with traditional chiral organic systems, inorganic quantum dots provide superior optical stability, broader spectral tunability, and stronger excitonic emission, making them highly attractive for practical applications in chiral photonics, spintronics, information encryption, and circularly polarized optoelectronic devices. Despite significant progress, several critical challenges remain. First, the microscopic origin of chirality transfer from chiral ligands to inorganic cores is still not fully understood, especially in systems where no obvious structural asymmetry is observed. In particular, the dominant mechanisms, including ligand – surface coordination asymmetry, electronic coupling – induced spin polarization, and symmetry breaking during nucleation and growth remain under debate and may vary significantly across different material systems. Second, achieving the simultaneous optimization of high photoluminescence quantum yield and large g_{lum} values remains difficult, as these two parameters are often mutually constrained. This trade-off typically arises because strong surface functionalization or chiral ligand coverage can enhance chiroptical activity but may introduce surface trap states or perturb exciton recombination pathways, thereby reducing radiative efficiency. Conversely, highly passivated or defect-free quantum dots often exhibit excellent PLQY but weak chiral asymmetry due to insufficient symmetry breaking at the surface or interface. Third, improving the long-term stability of chiral quantum dots, particularly in perovskite and carbon-dot systems, is necessary for practical device applications. Instability issues are often associated with ligand desorption, ion migration, moisture/oxygen sensitivity, and structural reconstruction under thermal or optical excitation, which can lead to gradual decay of both emission intensity and chiroptical signals over time. Moreover, expanding CPL-active materials into the near-infrared region will be particularly important for biological imaging, telecommunications, and spin-photon interfaces. However, achieving efficient NIR CPL emission is challenging due to inherently lower bandgap-related radiative efficiencies and increased non-radiative decay channels in narrow-bandgap semiconductor systems, requiring more sophisticated band engineering and surface-state control strategies.

In addition to improving chiroptical performance, the long-term stability of CPL-active inorganic nanomaterials is also critical for practical applications. Current studies have shown that some material systems, particularly perovskite nanocrystals and certain carbon-dot-based materials, may suffer from ligand desorption, surface oxidation, ion migration,

or structural reconstruction under environmental or optical stress, leading to gradual degradation of luminescence and CPL activity. To address these issues, several strategies including core/shell engineering, multidentate ligand passivation, polymer encapsulation, and interface stabilization have been explored to improve both optical and chiroptical stability.

Overall, the continued exploration of structure and property relationships will not only deepen the fundamental understanding of chiral inorganic nanomaterials but also accelerate the development of next-generation CPL-active optoelectronic systems with high efficiency, strong stability, and practical applicability. In this context, future studies combining advanced in situ characterization techniques, theoretical modeling of chiral excitonic states, and rational interface engineering may help further clarify structure – property relationships and support CPL-active inorganic nanomaterials in optoelectronics, spintronics, sensing, and biological applications.

Response Letter is available for this paper at: http://cjl. lightpublishing. cn/thesisDetails#10. 37188/CJL. 20220***(20220***为文章稿号).

References:

[1] Sánchez-Carnerero E. M., Agarrabeitia A. R., Moreno F., *et al.*, Circularly Polarized Luminescence from Simple Organic Molecules[J]. *Chemistry – A European Journal*, 2015, 21(39): 13488-13500.

[2] Zhang Y., Yu S., Han B., *et al.*, Circularly polarized luminescence in chiral materials[J]. *Matter*, 2022, 5(3): 837-875.

[3] Wang X., Yan W., Pang D.-W., *et al.*, From synthesis to chiroptical activities: advancements in circularly polarized luminescent inorganic quantum dots[J]. *Nanoscale*, 2025, 17(1): 158-186.

[4] Ma W., Xu L., de Moura A. F., *et al.*, Chiral Inorganic Nanostructures[J]. *Chemical Reviews*, 2017, 117(12): 8041-8093.

[5] Kotov N. A., Liz-Marzán L. M., Weiss P. S., NanostructuresChiral: New Twists[J]. *ACS Nano*, 2021, 15(8): 12457-12460.

[6] Tiwari M. P., Prasad A., Molecularly imprinted polymer based enantioselective sensing devices: A review[J]. *Analytica Chimica Acta*, 2015, 853: 1-18.

[7] Schadt, M., Liquid crystal material and liquid crystal displays[J]. *Annual Review of Materials Research*, 2003, 27: 305-379.

[8] Farshchi R., Ramsteiner M., Herfort J., *et al.*, Optical communication of spin information between light emitting diodes [J]. *Applied Physics Letters*, 2011, 98(16): 162508.

[9] Liu T., Shi W., Tang W., *et al.*, High Responsivity Circular Polarized Light Detectors based on Quasi Two-Dimensional Chiral Perovskite Films[J]. *ACS Nano*, 2022, 16(2): 2682-2689.

[10] Lin S., Tang Y., Kang W., *et al.*, Photo-triggered full-color circularly polarized luminescence based on photonic capsules for multilevel information encryption[J]. *Nat Commun*, 2023, 14(1): 3005.

[11] Song F., Xu Z., Zhang Q., *et al.*, Highly Efficient Circularly Polarized Electroluminescence from Aggregation-Induced Emission Luminogens with Amplified Chirality and Delayed Fluorescence[J]. *Advanced Functional Materials*, 2018, 28: 1800051.

[12] Dong J., Xu L., Qu A., *et al.*, Chiral Inorganic Nanomaterial-Based Diagnosis and Treatments for Neurodegenerative Diseases[J]. *Advanced Materials*, 2025, 37(11): 2418723.

[13] Gong Z.-L., Zhu X., Zhou Z., *et al.*, Frontiers in circularly polarized luminescence: molecular design, self-assembly, nanomaterials, and applications[J]. *Science China Chemistry*, 2021, 64.

[14] 刘培朝, 张怀芳, 周宾倩, *et al.*, II~VI族半导体纳米晶体的手性研究前沿[J]. 中国科学 : 化学, 2024, 54(8): 1337-1351.

[15] Su X., Fang S., Zhang Y., *et al.*, Shining Light on Group II – VI Chiral Quantum Dots: Synthesis, Chirality Induction, and Applications[J]. *ACS Applied Materials & Interfaces*, 2026, 18(9): 13344-13370.

[16] Moloney M. P., Gun′ko Y. K., Kelly J. M., Chiral highly luminescent CdS quantum dots[J]. *Chemical Communications*, 2007(38):3900-3902.

[17] Zhang Y., Hu L., Sun Y., *et al.*, One-step synthesis of chiral carbon quantum dots and their enantioselective recognition [J]. *RSC Advances*, 2016,6(65):59956-59960.

[18] Georgieva Z. N., Bloom B. P., Ghosh S., *et al.*, Imprinting Chirality onto the Electronic States of Colloidal Perovskite Nanoplatelets[J]. *Adv Mater*, 2018,30(23):e1800097.

[19] Cai J., Liu A.-A., Shi X.-H., *et al.*, Enhancing Circularly Polarized Luminescence in Quantum Dots through Chiral Coordination-Mediated Growth at the Liquid/Liquid Interface[J]. *Journal of the American Chemical Society*, 2023,145(44):24375-24385.

[20] Hu H., Zhang N., Zhang W., *et al.*, Synthesis of oleophilic chiral chalcogenide quantum dots via ligand engineering [J]. *Nano Research*, 2026,19(4):94908217.

[21] Yang J. T., 2 - OPTICAL ROTATORY DISPERSION AND CIRCULAR DICHROISM, in A Laboratory Manual of Analytical Methods of Protein Chemistry, P. *Alexander and H. P. Lundgren*, Editors. 1969, Pergamon. p. 23-92.

[22] Barron L. D., Molecular Light Scattering and Optical Activity. *2 ed.* 2004, Cambridge: Cambridge University Press.

[23] Johnson W. C., [20] Analysis of circular dichroism spectra, in Methods in Enzymology. 1992, Academic Press. p. 426-447.

[24] Kaizaki S., Applications of Electronic Circular Dichroism to Inorganic Stereochemistry, in Comprehensive Chiroptical Spectroscopy. 2012. p. 449-471.

[25] Stalder M., Schadt M., Linearly polarized light with axial symmetry generated by liquid-crystal polarization converters [J]. *Opt Lett*, 1996,21(23):1948-50.

[26] Nikolova L., Todorov T., Ivanov M., *et al.*, Polarization holographic gratings in side-chain azobenzene polyesters with linear and circular photoanisotropy[J]. *Appl. Opt.*, 1996,35(20):3835-3840.

[27] Carr R., Evans N. H., Parker D., Lanthanide complexes as chiral probes exploiting circularly polarized luminescence [J]. *Chemical Society Reviews*, 2012,41(23):7673-7686.

[28] Sang Y., Han J., Zhao T., *et al.*, Circularly Polarized Luminescence in Nanoassemblies: Generation, Amplification, and Application[J]. *Advanced Materials*, 2020,32(41):1900110.

[29] Wang X., Wang Y., Gao W., *et al.*, Polarization-Sensitive Halide Perovskites for Polarized Luminescence and Detection: Recent Advances and Perspectives[J]. *Advanced Materials*, 2021,33(12):2003615.

[30] Albano G., Pescitelli G., Di Bari L., Chiroptical Properties in Thin Films of π-Conjugated Systems[J]. *Chemical Reviews*, 2020,120(18):10145-10243.

[31] Train C., Gruselle M., Verdaguer M., The fruitful introduction of chirality and control of absolute configurations in molecular magnets[J]. *Chemical Society Reviews*, 2011,40(6):3297-3312.

[32] Ibanez J. G., Rincón M. E., Gutierrez-Granados S., *et al.*, Conducting Polymers in the Fields of Energy, Environmental Remediation, and Chemical – Chiral Sensors[J]. *Chemical Reviews*, 2018,118(9):4731-4816.

[33] Elliott S. D., Moloney M. P., Gun'ko Y. K., Chiral Shells and Achiral Cores in CdS Quantum Dots[J]. *Nano Letters*, 2008,8(8):2452-2457.

[34] Govan J. E., Jan E., Querejeta A., *et al.*, Chiral luminescent CdS nano-tetrapods[J]. *Chemical Communications*, 2010,46(33):6072-6074.

[35] Zhou Y., Yang M., Sun K., *et al.*, Similar Topological Origin of Chiral Centers in Organic and Nanoscale Inorganic Structures: Effect of Stabilizer Chirality on Optical Isomerism and Growth of CdTe Nanocrystals[J]. *Journal of the American Chemical Society*, 2010,132(17):6006-6013.

[36] Zhou Y., Zhu Z., Huang W., *et al.*, Optical Coupling Between Chiral Biomolecules and Semiconductor Nanoparticles: Size-Dependent Circular Dichroism Absorption[J]. *Angewandte Chemie International Edition*, 2011,50(48):11456-11459.

[37] Sun M., Xu L., Qu A., *et al.*, Site-selective photoinduced cleavage and profiling of DNA by chiral semiconductor nanoparticles[J]. *Nature Chemistry*, 2018,10(8):821-830.

[38] Wu T., Kapitán J., Mašek V., *et al.*, Detection of Circularly Polarized Luminescence of a Cs-EuIII Complex in Raman

Optical Activity Experiments[J]. *Angewandte Chemie International Edition*, 2015,54(49):14933-14936.

[39] Li G., Fei X., Liu H., *et al.*, Fluorescence and Optical Activity of Chiral CdTe Quantum Dots in Their Interaction with Amino Acids[J]. *ACS Nano*, 2020,14(4):4196-4205.

[40] Smith A. M., Duan H., Mohs A. M., *et al.*, Bioconjugated quantum dots for in vivo molecular and cellular imaging[J]. *Advanced Drug Delivery Reviews*, 2008,60(11):1226-1240.

[41] Qu S., Jia Q., Li Z., *et al.*, Chiral NIR-II fluorescent Ag2S quantum dots with stereospecific biological interactions and tumor accumulation behaviors[J]. *Science Bulletin*, 2022,67(12):1274-1283.

[42] Tohgha U., Varga K., Balaz M., Achiral CdSe quantum dots exhibit optical activity in the visible region upon post-synthetic ligand exchange with d- or l-cysteine[J]. *Chemical Communications*, 2013,49(18):1844-1846.

[43] Tohgha U., Deol K. K., Porter A. G., *et al.*, Ligand Induced Circular Dichroism and Circularly Polarized Luminescence in CdSe Quantum Dots[J]. *ACS Nano*, 2013,7(12):11094-11102.

[44] Choi J. K., Haynie B. E., Tohgha U., *et al.*, Chirality Inversion of CdSe and CdS Quantum Dots without Changing the Stereochemistry of the Capping Ligand[J]. *ACS Nano*, 2016,10(3):3809-3815.

[45] Cheng J., Hao J., Liu H., *et al.*, Optically Active CdSe-Dot/CdS-Rod Nanocrystals with Induced Chirality and Circularly Polarized Luminescence[J]. *ACS Nano*, 2018,12(6):5341-5350.

[46] Hao J., Li Y., Miao J., *et al.*, Ligand-Induced Chirality in Asymmetric CdSe/CdS Nanostructures: A Close Look at Chiral Tadpoles[J]. *ACS Nano*, 2020,14(8):10346-10358.

[47] Hao J., Zhao F., Wang Q., *et al.*, Optically Active CdSe/CdS Nanoplatelets Exhibiting Both Circular Dichroism and Circularly Polarized Luminescence[J]. *Advanced Optical Materials*, 2021,9(20):2101142.

[48] Merg A. D., Boatz J. C., Mandal A., *et al.*, Peptide-Directed Assembly of Single-Helical Gold Nanoparticle Superstructures Exhibiting Intense Chiroptical Activity[J]. *Journal of the American Chemical Society*, 2016, 138(41): 13655-13663.

[49] Sharma J., Chhabra R., Cheng A., *et al.*, Control of Self-Assembly of DNA Tubules Through Integration of Gold Nanoparticles[J]. *Science*, 2009,323(5910):112-116.

[50] Li C., Jin X., Zhao T., *et al.*, Optically active quantum dots with induced circularly polarized luminescence in amphiphilic peptide dendron hydrogel[J]. *Nanoscale Advances*, 2019,1(2):508-512.

[51] Wang Y., Wan K., Pan F., *et al.*, Bamboo-like π-Nanotubes with Tunable Helicity and Circularly Polarized Luminescence[J]. *Angewandte Chemie International Edition*, 2021,60(30):16615-16621.

[52] Jana S., de Frutos M., Davidson P., *et al.*, Ligand-induced twisting of nanoplatelets and their self-assembly into chiral ribbons[J]. *Science Advances*,3(9):e1701483.

[53] Chen L., Hao C., Cai J., *et al.*, Chiral Self-Assembled Film from Semiconductor Nanorods with Ultra-Strong Circularly Polarized Luminescence[J]. *Angewandte Chemie International Edition*, 2021,60(50):26276-26280.

[54] Kühnle A., Linderoth T. R., Hammer B., *et al.*, Chiral recognition in dimerization of adsorbed cysteine observed by scanning tunnelling microscopy[J]. *Nature*, 2002,415(6874):891-893.

[55] Xiang Z.-L., Tan Q.-H., Zhu T., *et al.*, High-performance 1D CsPbBr3/CdS photodetectors[J]. *Rare Metals*, 2024,43(11):5932-5942.

[56] Zhao Y., Askarpour A. N., Sun L., *et al.*, Chirality detection of enantiomers using twisted optical metamaterials[J]. *Nature Communications*, 2017,8(1):14180.

[57] Mukhina M. V., Korsakov I. V., Maslov V. G., *et al.*, Molecular Recognition of Biomolecules by Chiral CdSe Quantum Dots[J]. *Scientific Reports*, 2016,6(1):24177.

[58] Gao F., Ma S., Xiao X., *et al.*, Sensing tyrosine enantiomers by using chiral CdSe/CdS quantum dots capped with N-acetyl-l-cysteine[J]. *Talanta*, 2017,163:102-110.

[59] Fan X., Jiang L., Liu Y., *et al.*, Chiral CQD-based PL and CD sensors for high sensitive and selective detection of heavy metal ions[J]. *Optical Materials*, 2023,137:113620.

[60] Wu P., Zhao T., Wang S., *et al.*, Semicondutor quantum dots-based metal ion probes[J]. *Nanoscale*, 2014,6(1):43-64.

[61] Wang X., Hao J., Cheng J., *et al.*, Chiral CdSe nanoplatelets as an ultrasensitive probe for lead ion sensing[J]. *Na-*

noscale, 2019,11(19):9327-9334.

[62] Tedsana W., Tuntulani T., Ngeontae W., A circular dichroism sensor for Ni2+ and Co2+ based on l-cysteine capped cadmium sulfide quantum dots[J]. *Analytica Chimica Acta*, 2015,867:1-8.

[63] Li Z., Li W., Li D., *et al.*, Circularly polarized light emission and detection by chiral inorganic semiconductors[J]. *Frontiers of Optoelectronics*, 2024,17(1):15.

[64] Duan T., Ai J., Chen S., *et al.*, Chiral CdSe/CdS quantum dot (in rod)-light-emitting diodes with circularly polarized electroluminescence[J]. *Nano Research*, 2022,15(10):9573-9577.

[65] Naaman R., Waldeck D. H., Spintronics and Chirality: Spin Selectivity in Electron Transport Through Chiral Molecules[J]. *Annual Review of Physical Chemistry*, 2015,66:263-281.

[66] Ben Dor O., Yochelis S., Radko A., *et al.*, Magnetization switching in ferromagnets by adsorbed chiral molecules without current or external magnetic field[J]. *Nature Communications*, 2017,8(1):14567.

[67] Bloom B. P., Kiran V., Varade V., *et al.*, Spin Selective Charge Transport through Cysteine Capped CdSe Quantum Dots[J]. *Nano Letters*, 2016,16(7):4583-4589.

[68] Das S., Mondal S., Ghosh D., Carbon quantum dots in bioimaging and biomedicines[J]. *Frontiers in Bioengineering and Biotechnology*, 2024, Volume 11 - 2023.

[69] Pourmadadi M., Rahmani E., Rajabzadeh-Khosroshahi M., *et al.*, Properties and application of carbon quantum dots (CQDs) in biosensors for disease detection: A comprehensive review[J]. *Journal of Drug Delivery Science and Technology*, 2023,80:104156.

[70] You W., Zou W., Jiang S., *et al.*, Fluorescent carbon quantum dots with controllable physicochemical properties fantastic for emerging applications: A review[J]. *Carbon Neutralization*, 2024,3(2):245-284.

[71] Han Z., Wu Q., Lv X., *et al.*, Recycling Waste Rubber Into Single-Walled Carbon Nanotubes: Narrow Chirality Distribution and Hydrogen Byproduct[J]. *Carbon Neutralization*, 2025,4(5):e70059.

[72] Zhang M., Hu L., Wang H., *et al.*, One-step hydrothermal synthesis of chiral carbon dots and their effects on mung bean plant growth[J]. *Nanoscale*, 2018,10(26):12734-12742.

[73] Hu L., Sun Y., Zhou Y., *et al.*, Nitrogen and sulfur co-doped chiral carbon quantum dots with independent photoluminescence and chirality[J]. *Inorganic Chemistry Frontiers*, 2017,4(6):946-953.

[74] Malishev R., Arad E., Bhunia S. K., *et al.*, Chiral modulation of amyloid beta fibrillation and cytotoxicity by enantiomeric carbon dots[J]. *Chemical Communications*, 2018,54(56):7762-7765.

[75] Döring A., Ushakova E., Rogach A. L., Chiral carbon dots: synthesis, optical properties, and emerging applications[J]. *Light: Science & Applications*, 2022,11(1):75.

[76] Suzuki N., Wang Y., Elvati P., *et al.*, Chiral Graphene Quantum Dots[J]. *ACS Nano*, 2016,10(2):1744-1755.

[77] Das A., Arefina I. A., Danilov D. V., *et al.*, Chiral carbon dots based on l/d-cysteine produced via room temperature surface modification and one-pot carbonization[J]. *Nanoscale*, 2021,13(17):8058-8066.

[78] Lin J., Liu R., Chen P., *et al.*, Stimulating and harnessing circularly polarized luminescence of helically assembled carbonized polymer dots via interfacial dynamics[J]. *Aggregate*, 2023,4(4):e311.

[79] Xu L., Zhang H., Cui Y., *et al.*, Magnetic modulation on chiroptical activities of nematically assembled carbon dots[J]. *Journal of Colloid and Interface Science*, 2025,678:409-416.

[80] Ghosh A., Parasar B., Bhattacharyya T., *et al.*, Chiral carbon dots derived from guanosine 5′-monophosphate form supramolecular hydrogels[J]. *Chemical Communications*, 2016,52(74):11159-11162.

[81] Wang Y., Yu L., Lv T., *et al.*, Chiral carbonized polymer dots simultaneously achieving solid state luminescence and circularly polarized luminescence[J]. *Dyes and Pigments*, 2023,220:111685.

[82] Wang D., Zhang Z., Yan X., *et al.*, Construction of a circularly polarized luminescence sensor based on self-assembly of carbon dots and G-quartet chiral nanofibers[J]. *Nanoscale*, 2025,17(3):1342-1349.

[83] Zhang Z., Wang D., Yan X., *et al.*, Efficient chiral hydrogel template based on supramolecular self-assembly driven by chiral carbon dots for circularly polarized luminescence[J]. *Journal of Colloid and Interface Science*, 2024,674:576-586.

[84] Ma W., Lu D., Liu J., *et al.*, Multicolor circularly polarized luminescence from chiral carbon dots and cellulose nanocrystals assemblies for visual polarization detection[J]. *Chemical Engineering Journal*, 2024,495:153453.

[85] Billing D. G., Lemmerer A., Bis-[(S)-β-phenethyl-ammonium] tri-bromo-plumbate(II)[J]. *Acta Crystallographica Section E*, 2003, 59(6): m381-m383.

[86] Lemmerer A., Billing David G., Inorganic-organic hybrids incorporating a chiral cyclic ammonium cation[J]. *South African Journal of Chemistry*, 2013, 66(1): 1.

[87] Ahn J., Lee E., Tan J., *et al.*, A new class of chiral semiconductors: chiral-organic-molecule-incorporating organic – inorganic hybrid perovskites[J]. *Materials Horizons*, 2017, 4(5): 851-856.

[88] Chen C., Gao L., Gao W., *et al.*, Circularly polarized light detection using chiral hybrid perovskite[J]. *Nat Commun*, 2019, 10(1): 1927.

[89] Di Nuzzo D., Cui L., Greenfield J. L., *et al.*, Circularly Polarized Photoluminescence from Chiral Perovskite Thin Films at Room Temperature[J]. *ACS Nano*, 2020, 14(6): 7610-7616.

[90] Shen H., Gong X., Yang Y., *et al.*, Chemically Tailored Organic Ammonium Salts for Integrated Regulation of CsPbI3 Perovskite Solar Cells[J]. *Carbon Neutralization*, 2026, 5(1): e70104.

[91] Billing D. G., Lemmerer A., Synthesis and crystal structures of inorganic – organic hybrids incorporating an aromatic amine with a chiral functional group[J]. *CrystEngComm*, 2006, 8(9): 686-695.

[92] Yuan C., Li X., Semin S., *et al.*, Chiral Lead Halide Perovskite Nanowires for Second-Order Nonlinear Optics[J]. *Nano Letters*, 2018, 18(9): 5411-5417.

[93] Long G., Zhou Y., Zhang M., *et al.*, Theoretical Prediction of Chiral 3D Hybrid Organic – Inorganic Perovskites[J]. *Advanced Materials*, 2019, 31(17): 1807628.

[94] He T., Li J., Li X., *et al.*, Spectroscopic studies of chiral perovskite nanocrystals[J]. *Applied Physics Letters*, 2017, 111(15): 151102.

[95] Shi Y., Duan P., Huo S., *et al.*, Endowing Perovskite Nanocrystals with Circularly Polarized Luminescence[J]. *Advanced Materials*, 2018, 30: 1705011.

[96] Wang C.-T., Chen K., Xu P., *et al.*, Fully Chiral Light Emission from CsPbX3 Perovskite Nanocrystals Enabled by Cholesteric Superstructure Stacks[J]. *Advanced Functional Materials*, 2019, 29.

[97] Ma S., Jung Y.-K., Ahn J., *et al.*, Elucidating the origin of chiroptical activity in chiral 2D perovskites through nano-confined growth[J]. *Nature Communications*, 2022, 13(1): 3259.

[98] Liu H., Portniagin A. S., Tang B., *et al.*, Helical Perovskite Nanowires with Strong Circularly Polarized Luminescence Self-Assembled from Red-Emitting CsPbI₃ Quantum Dots Following Chiral Ligand Exchange[J]. *ACS nano*, 2025, 19(18): 17774-17784.

[99] Zeng Z., Wang D.-B., Fang X., *et al.*, Review of 2D Bi2X3 (X = S, Se, Te): from preparation to photodetector[J]. *Rare Metals*, 2024, 43(6): 2349-2370.

[100] Kim J., Yoon H., Sohn I., *et al.*, Near-infrared self-powered RuS2xSe2−2x alloy photodetector via chemical vapor deposition RuSe2 and post-sulfurization process[J]. *Rare Metals*, 2025, 44(6): 4050-4060.

[101] Ye T., Wang Z., Ma S., *et al.*, Flexible Perovskite Solar Cells: Low Temperature Processing, Material Design, and Pathways to Scalable Green Photovoltaics[J]. *Carbon Neutralization*, 2025, 4(5): e70047.

[102] Zheng Y.-Y., Wang H.-B., Wang S., *et al.*, Linearly polarized photodetectors based on low-dimensional perovskites: theory, material, and device[J]. *Rare Metals*, 2025, 44(10): 6839-6864.

[103] Guo Q., Wang X.-J., Wang L., *et al.*, Ultrathin BiOCl crystals grown in highly disordered vapor micro-turbulence for deep ultraviolet photodetectors[J]. *Rare Metals*, 2024, 43(11): 5921-5931.

[104] Liu Q., Wei Q., Ren H., *et al.*, Circular polarization-resolved ultraviolet photonic artificial synapse based on chiral perovskite[J]. *Nat Commun*, 2023, 14(1): 7179.

[105] Yang L., Gao Y., Wang Z., *et al.*, Spin detector for panchromatic circularly polarized light detection[J]. *Nature Communications*, 2025, 16(1): 4161.

[106] Kim Y.-H., Zhai Y., Lu H., *et al.*, Chiral-induced spin selectivity enables a room-temperature spin light-emitting diode[J]. *Science*, 2021, 371: 1129-1133.

[107] Li D., Liu X., Wu W., *et al.*, Chiral Lead-Free Hybrid Perovskites for Self-Powered Circularly Polarized Light Detection[J]. *Angewandte Chemie International Edition*, 2021, 60(15): 8415-8418.

[108] Yao J., Wang Z., Huang Y., *et al.*, Efficient Green Spin Light-Emitting Diodes Enabled by Ultrafast Energy- and Spin-Funneling in Chiral Perovskites[J]. *Journal of the American Chemical Society*, 2024, 146(20): 14157-14165.

[109] He S., Lin W., Yu D., *et al.*, Perovskite spin light-emitting diodes with simultaneously high electroluminescence dissymmetry and high external quantum efficiency[J]. *Nature Communications*, 2025, 16(1): 2201.

周宾倩(1999-),女,河南周口人,博士研究生,2022年于河南师范大学获得学士学位,主要从事手性无机纳米材料合成及手性效应的研究。
E-mail: zhoubq@stu.hubu.edu.cn

郝俊杰(1987-),男,河南林州人,博士,副教授,硕士生导师,2020年于法国波尔多大学获得博士学位,主要从事低维量子材料及其光电芯器件研究。
E-mail: haojunjie@sztu.edu.cn

程佳吉(1988-),男,湖北武汉人,博士,副教授,硕士生导师,2015年于法国波尔多大学获得博士学位,主要从事多层次凝聚态纳米材料的手性构筑以及手性无机纳米材料立体构象的纳米光子学研究。
E-mail: jiajicheng@hubu.edu.cn